Photonic Sensors (2011) Vol. 1, No. 4: 295–322

DOI: 10.1007/s13320-011-0041-4 **Photonic Sensors**

Review

Applied Optics to Engineering Photonics: a Retrospective

Ralph P. TATAM

Department of Engineering Photonics, School of Engineering, Cranfield University, Cranfield, Bedford, MK43 0AL, UK

*Corresponding author: Ralph P. TATAM E-mail: r.p.tatam@cranfield.ac.uk

Abstract: This paper provides a short overview of the time I spent as a member of the Applied Optics Group at the University of Kent (1985–1989) followed by a review of my research during my time at Cranfield University (1989 to date).

Keywords: Optical fiber sensors, optical instrumentation, laser velocimetry, speckle interferometry, fiber Bragg gratings, long period fiber gratings, optical gas sensing, optical coherence tomography, flow measurement, coherent fiber optic bundles

1. Introduction

I was a member of the Applied Optics Group (AOG) at the University of Kent, led by Prof. David Jackson, from February 1985 until March 1989. My initial appointment was as a research fellow employed on a UK Science and Engineering Research Council (SERC) grant titled interferometric guided wave sensors. After 2 years I was appointed as a temporary lecturer within the Physics Laboratory where one of my major activities was to manage a recently awarded teaching company scheme (TCS), funded by the SERC, in association with Sifam Ltd., UK. The TCS scheme was established to assist technology transfer from universities to companies and this particular program was to develop a novel optical fiber current sensor for the electricity supply industry; more details of this are in Section 2. In April 1989 I took up a permanent lectureship at Cranfield Institute of Technology, now Cranfield University. My brief was to set up a new research group in the area of optical and optical fiber instrumentation. In the early days the aim was to develop novel optical instrumentation which could be used to make measurements on the full scale gas turbine compressor facilities at Cranfield, for example fiber optic laser velocimetry instrumentation, described in more detail later. Locating an optical instrumentation research activity within an engineering and applied science environment, that is, locating the instrumentation research activity in the same environment as many of the potential users of the technology proved inspirational to me and benefited, I hope, the researchers from the many disciplines with whom my team and I have had the pleasure of collaborating. As a consequence my research interests have developed across many application areas over the years, some of which are described in Section 3, and can best be summarized as the use of optical and optical fiber based instrumentation to solve measurement challenges within engineering, biomedical and applied science applications.

This paper provides a short overview of my research whilst a member of the AOG at the University of Kent followed by a review of my research interests at Cranfield.

Received: 24 June 2011 / Revised version: 28 July 2011

2. Research in the AOG (1985–1989)

As a member of the AOG (Fig. 1) the majority of the research projects with which I was involved were based on controlling the state of polarization (SOP) of an optical beam using both singlemode and birefringent optical fiber. Initial work focused on controlling the azimuth of a linearly polarized light beam using bulk optic interferometers and introducing a phase change between two circularly polarized beams of light of orthogonal polarization. High speed operation was obtained using a Bragg cell in one path of the interferometer [1] and fiber based modulation using fiber wrapped around piezoelectric modulators [1, 2]. These polarization state control schemes were used as signal processing techniques in a range of applications including light scattering [1], the measurement of optical activity [2], laser velocimetry [3] and Faraday rotation electric/magnetic field measurement [4–8]. The birefringent optical fiber approach to SOP control was extended to show that all possible polarization states could be accessed in a controllable fashion by using two lengths of birefringent optical fiber with their eigenaxes orientated at 45° with respect to each other [9]. Linearly polarized, or circularly polarized, light coupled into the first length of optical fiber orientated at 45° with respect to the eigenaxes can be converted into any SOP at the exit of the second length of optical fiber by changing the relative retardation between the polarization eigenmodes in each length of fiber, i.e. it is possible to access any point on the surface of the Poincarė sphere. By adding a third length of birefringent optical fiber also with its eigenaxes orientated at 45° with respect to the previous length of fiber it is possible to convert any input SOP to any output SOP.

The measurement of electric current/magnetic field using the Faraday effect led to a number of projects within the AOG, of which many being investigated at that time were summarized in [7], and I was involved with a collaboration with Sifam Ltd. (Torquay, Devon, UK) to design and build a fiber optic instrument for measuring electric current for electricity supply protection.

Fig. 1 Some members of the AOG in March 1987 [from left to right: Prof. David Jackson, Prof. Ralph Tatam (now at Cranfield University, UK), Prof. Julian Jones (now at Heriot Watt University, Edinburgh, UK), Prof. Faramarz Farahi (now at University of North Carolina at Charlotte, USA), Dr. David Webb (now at Aston University, UK), Dr. Mike Berwick (now at Brunel University, UK), Prof. Chris Pannell (now at Gooch and Housego, USA), Mr. Roy Povey (now retired), Dr. David Hughes, Dr. Trevor Newson (now at Southampton University, UK), Dr. Awad Gerges (now at University of North Carolina at Charlotte, USA), and Dr. Nobu Takahashi (visitor from Himeji Institute of Technology, Hyogo, Japan)].

The rationale for this was that conventional current transformers were known to explode due to degradation in the electrical insulation used and there was therefore considerable interest in using optical methods that would be immune to this problem as well as offering additional advantages such as fast response time and a large measurement dynamic range as the fiber sensor didn't saturate, even at very large currents.

The technique we explored used coils of fiber possessing very low levels of intrinsic birefringence – spun fiber – and a novel arrangement of three polarisation analyzers orientated at 120° with respect to each other allowing the azimuth and ellipticity of the SOP to be determined but not the handedness. This scheme had the advantage of not requiring a beamsplitter, which tended to introduce unwanted birefringence into the propagating beam, and very simple alignment between the fiber and detector

assembly. In addition, the ability to measure the ellipticity enabled compensation for scale factor errors caused by linear birefringence in the fiber when the fiber was formed into a coil [8]. Figure 2 shows the prototype sensor that was constructed and installed at an electrical substation. Singlemode optical fiber was formed into a loop surrounding a current carrying conductor with the optoelectronic components contained in the box standing on the platform.

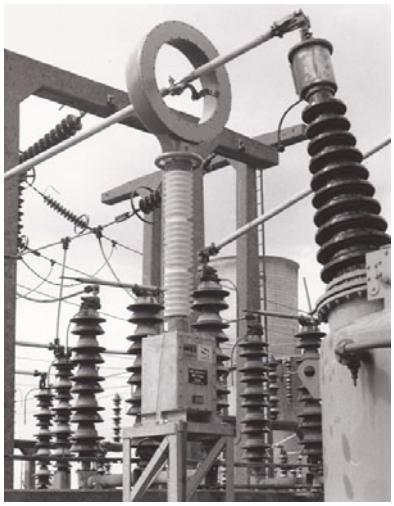

Fig. 2 Photo of prototype electric current measuring system developed under the TCS program with Sifam.

During this time we also started investigating the possibility of producing in-fiber frequency shifters with a view to replacing bulk optic devices such as Bragg cells as heterodyne signal processing elements in all-fiber sensor systems. The devices were based on coupling light between the eigenmodes in birefringent optical fiber using a travelling flexural wave in the fiber generated by coupling acoustic waves into the fiber using an acoustic horn [10, 11]. This work, which was led by Chris Pannell, with whom I also collaborated in investigating the application of birefringent fibers in laser velocimetry applications [3], achieved frequency shifts of about 800 kHz in birefringent fiber with a beatlength of about 1.2 mm. I also collaborated with Simon Waite at City University, to investigate the potential of birefringent optical fiber, configured as a polarimeter, embedded within woven glass reinforced plastic to detect strain changes and damage within the material [12]. We demonstrated that a simple processing scheme was applicable to recovering strain changes of 0.1%. For many of the projects using birefringent optical fiber there was a requirement to know the beatlength of the fiber. Fiber manufacturers generally only give a range of values and the beatlength is also wavelength dependent. We investigated measuring the beatlength visually by observing the light scattered from the fiber at 45° to the eigenaxes (Fig. 3), using a microscope. However, it is difficult to achieve precise measurements in practice since temperature fluctuations cause the pattern to move so that you have to hold your breath whilst making the measurements and this method only works for visible light.

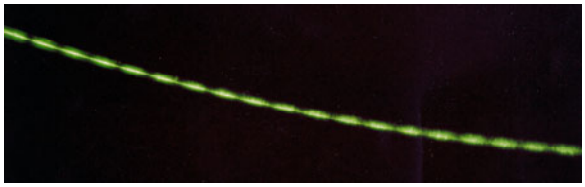

Fig. 3 Light scattered from a birefringent optical fiber guiding light from an argon ion laser (514.5 nm) in both polarization eigenmodes.

I worked with David Webb, then a PhD student, with whom I also worked on a interferometric refractometer [13], on a technique based on modulating the emission frequency of a laser diode to measure the optical pathlength difference between the orthogonal polarization eigenmodes in birefringent fiber [14] that measured the beatlength of about 8.5 m of York Technology highly birefringent (“bowtie”) fiber (HB600) to be (1.50 +/- 0.05) mm.

Chromatic dispersion in optical fibers is an important parameter to determine particularly for high speed telecommunications where it can be the limiting factor influencing performance. At this time Paul Merritt, a BT/SERC sponsored PhD student, was investigating white light interferometry as a method to measure dispersion in short, lengths of

singlemode optical fiber. This required very careful experimentation as solid state broad band light sources were in their infancy with low output power, poor beam profile and not being fiber pigtailed. My contribution to this work was the computational analysis of the data which, combined with Paul's excellent experimental results, resulted in a resolution of about 7×10^{-5} ps·nm^{-1} in about 1-m length of fiber [15]. Interestingly, this paper received only 4 citations in the first 12 years following publication but has received an additional 30 [16] since 2002 of which 15 were in the last 2–3 years, reflecting the interest in photonic crystal fiber (PCF) and holey fibers and new techniques to measure their dispersion.

Finally, although the use of optical techniques and optical fibers in particular in biological applications has become more popular and indeed more recent work from the AOG has investigated biomedical applications of fiber Bragg grating sensors, it was much more in its infancy in the mid 1980's. We explored, in collaboration with a biochemist at the University of Kent (Guy Rollinson), the application of singlemode optical fibers to measure temperature changes in a microbial suspension [17] demonstrating that optical fiber interferometric sensing was capable of providing the sensitivity needed to measure temperature in biological applications.

3. Research at Cranfield (1989–2011)

As I indicated earlier my research work at Cranfield has been aimed at providing solutions to measurement problems in a range of application areas using optical, and in many cases, optical fiber based instrumentation techniques. Much of the research has been interdisciplinary and collaborative which has been challenging, enjoyable and a great learning experience. For ease of presentation I have divided the research up into several themes but in reality there is a lot of overlap between them and in many cases the division is somewhat artificial.

3.1 Laser velocimetry

One of my initial goals when I started at Cranfield was to investigate novel approaches for the measurement of flow within gas turbine engines and in particular gas turbine compressors, a major activity at Cranfield for many years led by Prof. Robin Elder. Although offering significant potential benefits, optical methods suffered in this application from a lack of optical access into the compressor and therefore the measurement of three orthogonal velocity components was very challenging. We initiated a program to investigate how we could obtain simultaneous 3-component measurements using optical fiber technology to minimize the instrument size and make it more readily deployable on the compressor rig. All the instrumentation developed was based on the Doppler shift of scattered light from moving particles entrained in the flow. The frequency shift, Δv , is given by (1):

$$\Delta v = \frac{v(\hat{o}-\hat{i})\cdot V}{c} \tag{1}$$

where v is the optical frequency, $\hat{o}$ and $\hat{i}$ are unit vectors in the observation and illumination directions respectively, V is the velocity vector, and c is the free space speed of light, (Fig. 4)

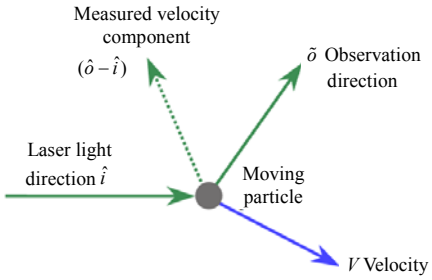

Fig. 4 Relationship between illumination and observation directions to the measured velocity component.

It is generally relatively straight forward to obtain the orthogonal velocity components that are perpendicular to the laser light direction using a Doppler difference configuration (Fig. 5), where two laser beams intersect to form a measurement volume. As a particle traverses the fringes formed in this volume light is scattered at a frequency dependent on the fringe spacing and the particle velocity.

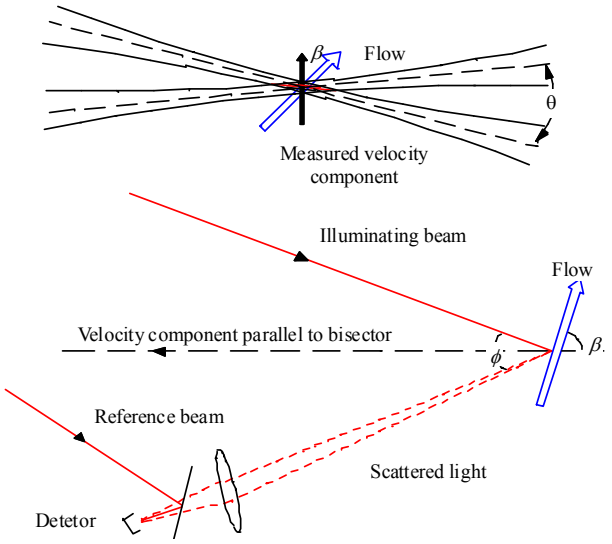

Fig. 5 Doppler difference configuration (top) and reference beam configuration (bottom) (β is the flow angle and ϕ is the angle between the incident beam and the observation direction).

However, the in-line velocity component, often called the "elusive 3rd component", is more challenging because a third Doppler difference channel cannot be incorporated due to lack of optical access. Several of our research programs investigated techniques to measure the in-line velocity component from a single optical head.

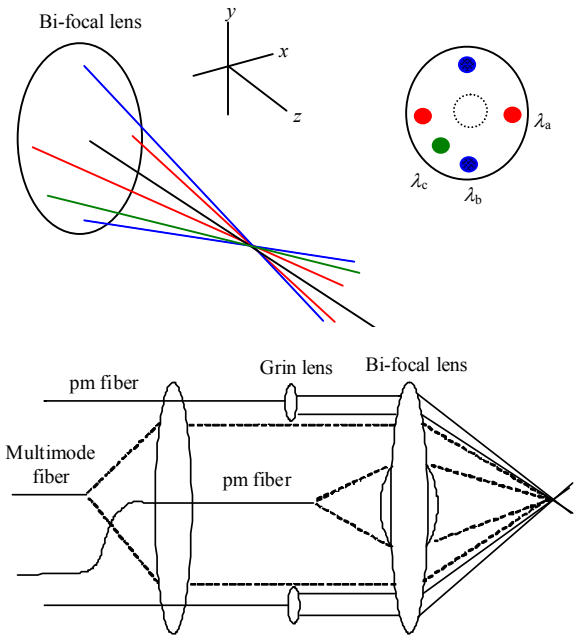

Fig. 6 Schematic of single-headed 3-component fiber optic laser velocimeter using two Doppler difference and one reference beam channel (λ_a, λ_b, λ_c represent the three different wavelengths used to discriminate the measurements).

A prototype fiber optic based 3-component laser velocimeter that we designed and constructed is shown in Fig. 6 [18]. The instrument consists of two Doppler difference measurement channels to measure the "x" and "y" velocity components and a fiber optic reference beam configuration is used to measure the in-line, "z", velocity component. Discrimination between channels is achieved by using different wavelengths for each measurement channel.

The periphery of a bifocal lens is used to focus light exiting from five birefringent optical fibers, used to maintain the SOP of the interfering beams, to form co-located measurement volumes. The center of the bifocal lens is used to couple the scattered light into a sixth birefringent optical fiber which forms the return path for the reference beam channel. The outside of the bifocal lens is also used to collect the scattered light and image it onto a multimode optical fiber.

The arrangement is similar to that we reported in [19] except a second fiber is used for the return path to shorten the measurement volume size in the "z" direction; the measurement volume size was 50 μm×50 μm×500 μm for the Doppler difference channels and 24 μm×24 μm×500 μm for the reference beam channel with a working distance of 200 mm. The optical head is shown in Fig. 7. The fibers in the probe are linked to a remote breadboard, shown schematically in Fig. 8, containing three high power, about 150 mW at about 800 nm, 810 nm and 820 nm, lasers with Blue-Sky^{TM} circulaser technology, a lens system bonded to the laser output window that removes the ellipticity and high divergence of the laser output into a collimated Gaussian beam, resulting in a coupling efficiency of about 60% into singlemode fiber, three avalanche photodiodes detectors (APDs), a diffraction grating to separate the wavelengths from the multimode fiber, three fiber-coupled Bragg cells that act as beamsplitters and frequency shifters to implement heterodyne signal processing and a

polarization preserving variable split ratio directional coupler, manufactured in my laboratory, used to optimize the signal to noise (S/N) ratio on the reference beam channel. This arrangement used a number of innovative technologies at the time, for example, circulaser technology combined with high power single frequency laser diodes, birefringent fiber coupled Bragg cells and a fiber optic reference beam channel constructed in birefringent fiber including the coupler. This technology was subsequently used to measure flow angles for gas turbine applications and incorporated in-fiber Bragg grating (FBG) stabilization of the laser diode emission frequency [20].

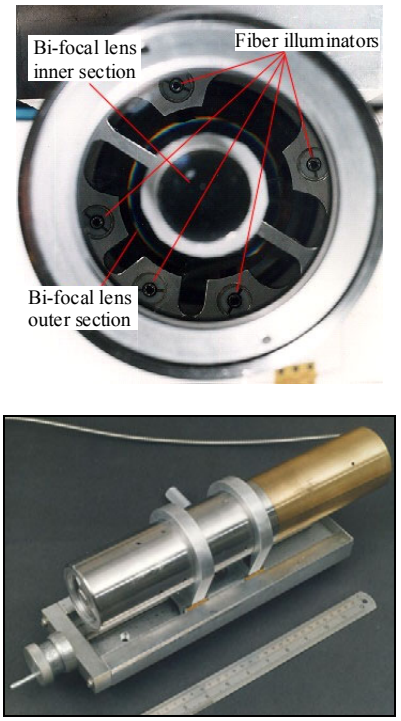

Fig. 7 Photo of single-headed three-component fiber optic laser Doppler velocimeter (the probe is 50 mm in diameter and about 300 mm long).

A difficulty with the use of the reference beam channel is that the geometry means the fringes are closely spaced and therefore for commercially available processors operating at 100 MHz–200 MHz the measured velocity component is limited to about 40 ms^{-1}, which is insufficient for high speed applications where flow velocities of hundreds of meters per second may need to be measured. This led to the investigation of alternative techniques to measure the in-line velocity component including a fiber optic Fabry-Perot interferometer formed using FBGs [21] and the use of an iodine absorption cell, discussed further below, as a narrow band edge filter [22]. These studies also resulted in a new optical heterodyne vibrometer arrangement based on a polarizing maintaining fiber coupler and remote processing interferometer that considerably reduced the alignment stability required from the bulk optic optical components [23]. Another issue with reference beam systems is optimizing the S/N ratio which requires careful balance of power between the received scattered light, generally very weak, mixing with a local reference beam. This is usually achieved by manual adjustment, as with the variable split ratio coupler described above. In [24] we described an alternative arrangement that used an FBG at the distal end of the fiber and a tuneable laser diode as the source. The reference beam was derived from the reflection from the FBG and the intensity of this reflection controlled by tuning the laser emission wavelength relative to the reflection spectrum of the FBG.

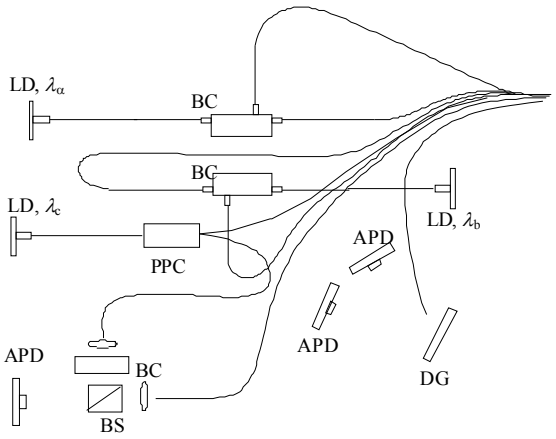

Fig. 8 Schematic of breadboard containing laser diodes (LD), Bragg cells (BC), diffraction grating (DG), APD detectors, beamsplitter (BS), and a polarization preserving directional coupler (PPC).

To reduce the optical complexity of the wavelength multiplexed arrangement described

above we investigated time-division multiplexing [19, 25]. In this arrangement a single high power laser diode was used and a network of fiber couplers split the output from the laser to form three measurement channels. The laser was pulsed at 33 MHz with a 20% duty cycle. Optical fiber delay lines were incorporated into each channel such that the optical pulse arrived in the measurement volume at different times for each channel. High speed acquisition followed by extraction of the pulses associated with each measurement channel and subsequent Fourier analysis enabled three-component velocity measurements to be made.

Although the instrumentation described above offers high spatial resolution it has the disadvantage that it takes significant amounts of time to map out flow fields, particularly for larger scale flow fields found in wind tunnel testing, for example. In addition there is increasing interest in techniques that are capable of providing information simultaneously from different regions of the flow enabling spatial features of the flow to be measured. The development of planar techniques has helped to address this issue. In planar flow measurement a region of the flow is illuminated with a laser beam conditioned to form a light sheet in the region of interest. The light scattered from particles entrained in the flow is imaged onto two-dimensional detector arrays, usually charge coupled devices (CCDs). The most developed planar flow measurement method is particle image velocimetry (PIV) in which two images of the flow are collected with a short time difference between them. Correlation techniques are then used to calculate the distance and direction a particle has moved. A single viewing direction and laser sheet results in the measurement of two velocity components in the plane of the sheet. The out-of-plane velocity component is more difficult to extract but techniques based on stereoscopic viewing have shown some success. Planar Doppler velocimetry (PDV) is capable of operating with a range of seeding densities, large flow fields and high speed flows (>100 m/s). Three components of velocity can be measured instantaneously or time-averaged depending on the laser source and image processing methods used. For a number of years we have been investigating PDV instrumentation and in particular how the use of optical fibers can improve the capability of the technique [26–32]. An experimental arrangement for PDV is shown in Fig. 9. The output laser is formed into a light sheet. This sheet is imaged onto two CCD cameras using the beamsplitter/mirror arrangement shown. One path is a frequency-to-intensity converter and the other path acts as a reference channel. An iodine vapor cell is often used as the frequency-to-intensity converter although more recently we have shown that it is possible to use a Mach-Zehnder interferometric approach [31, 32]. This later approach overcomes some of the limitations of the need for a gas cell such as a restricted choice of laser as it has to be tuneable across a gas absorption line and the transfer function is determined by the form of the gas absorption. In both cases measurements are made at two positions on the filter transfer function such that the signals can be normalized to remove intensity changes not due to Doppler frequency shifts. From the Doppler equation (1), it is evident that three components of velocity can be also obtained by detecting the light scattered from the particles in the light sheet from three different observation directions. A key part of our work in this field has been the introduction of coherent imaging fiber bundles into the instrumentation design. Figure 10 shows the arrangement using imaging fiber bundles and in this case a single CCD [29]. This has the advantage of removing the beamsplitter, which always exhibit residual birefringence thus compromising the intensity referencing, and ensures pixel registration between reference and signal images.

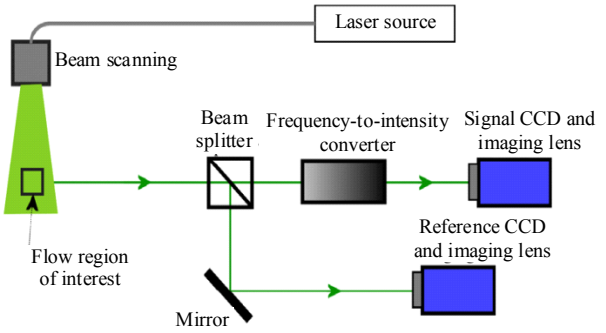

Fig. 9 A typical PDV arrangement for a single component measurement of velocity.

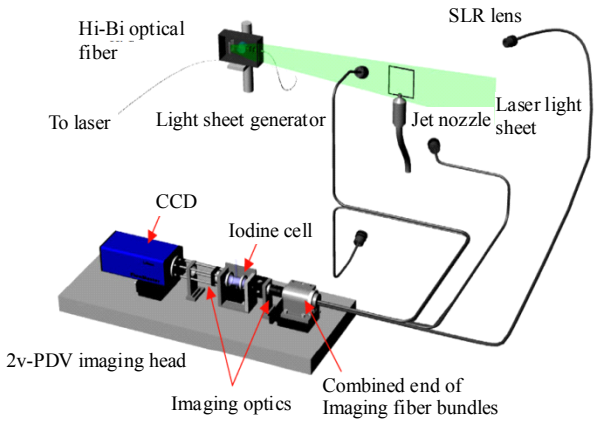

Fig. 10 PDV arrangement using 4 coherent imaging fiber bundles and a single CCD camera.

The fiber bundles used consist of 4 legs (600×500 fibers in each leg). Each fiber has an 8-μm-diameter core that is centered at 10 μm and each bundle is 4 m long. The bundles enable a range of optical imaging systems to be used. Figures 11–16 show the coherent imaging bundles, examples of imaging optics that can be used and photos of the laser velocimetry instrumention deployed on a gas turbine research compressor.

Fig. 11 Coherent imaging fiber bundles (600×500 fibers in each leg) in threaded mounts to enable couple to imaging systems.

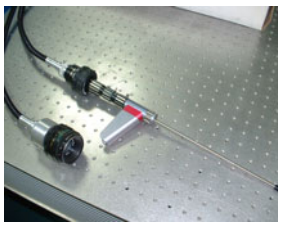

Fig. 12 Coherent imaging fiber bundles coupled to an industrial borescope (top) and a camera lens (bottom).

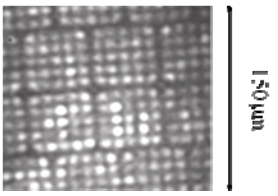

Fig. 13 Close up view of the individual fibers in the 5×5 sub-arrays of a wound fiber bundle.

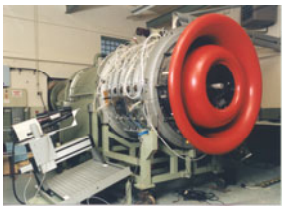

Fig. 14 4-stage axial research compressor at Cranfield with fiber optic laser anemometer mounted on left hand side.

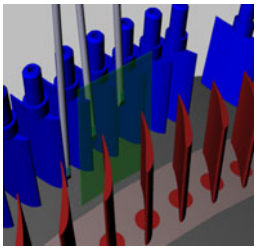

Fig. 15 Three commercially available imaging borescopes positioned between the rotors and stators within the compressor shown in Fig. 14.

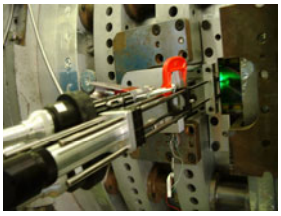

Fig. 16 Imaging bundles of PDV system coupled to borescopes mounted on the compressor shown in Fig. 14.

An example of a 3D flow field from a seeded air jet with a maximum velocity of about 100 $m \cdot s^{-1}$ is shown in Fig. 17. This approach has proved very flexible, achieving high quality flow field measurements and was adopted by the German Aerospace Center (DLR) for measurements in the European transonic wind tunnel [33] and by NASA [34].

As part of our experimental research program aimed at gas turbine engines we investigated the potential of optical methods to measure the condensation occurring in the air inlet of a gas turbine engine. The condensation causes as much as a 2% increase in the specific fuel consumption, causes inaccuracies during engine testing and is traditionally difficult to measure. An accurate measurement method would enable engines to be tested at any time reducing the cost of development programs. The system used a 10.6-μm CO_2 laser to measure the extinction coefficient due to Mie scattering from water droplets. At this wavelength

the extinction coefficient varies linearly with the liquid water content. We were able to demonstrate that the optical technique predicted a temperature rise in line with that of theory and non-optical experimental methods [35].

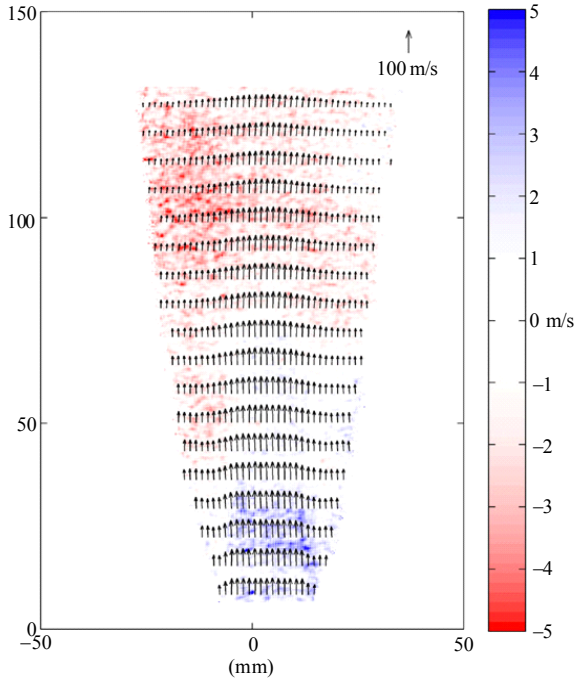

Fig. 17 3D flow measurements on a seeded air jet obtained using the instrumentation shown in Fig. 10 [vectors show the in-plane velocities (every 8th and 40th data point shown in the horizontal and vertical directions, respectively), and the values for the out-of-plane velocity are given by the bar on the right].

3.2 Speckle interferometry

An area of research that I became involved with shortly after starting at Cranfield was speckle interferometry. This is a technique that uses speckles, generated by the illumination of a surface that is rough on the scale of the wavelength of light with a coherent light source, to convey information about the state of the surface over an extended region of the surface. This includes the shape of the object, vibrational characteristics, deformation and surface strain and the ability to reveal sub surface cracks in, for example, pipes and composite materials. We have investigated both electronic speckle pattern interferometry (ESPI) and shearography, or speckle shearing interferometry. ESPI is based on an optical configuration similar to reference beam interferometry in that scattered light from the object surface is mixed with a local reference beam on a CCD camera. Figure 18 shows a fiber optic ESPI system illuminated with a laser diode [36]. Light is divided at the directional coupler usually 95% into the object beam and 5% into the reference beam. Light scattered from the object is imaged onto a CCD camera where it is mixed with a smooth reference beam from the reference arm. An example of a speckle image obtained is shown in Fig. 19. Interferometric fringes are obtained by correlating two speckle images obtained for either different physical locations of the object or different illumination conditions. These images are correlated, usually by subtraction, to form fringes with interferometric sensitivity. However, the phase information is lost in the correlation process and therefore optical processing techniques are required to recover the phase information so that the techniques may provide quantitative information. This is generally achieved by collecting a number of speckle images with a known phase difference between them and the combining these images with one of many algorithms available to recover the phase modulo 2π. Further digital image processing is then used to “unwrap” the images to produce quantitative maps of shape, strain and vibration for example. Our initial work looked at signal processing methods to recover the phase information in fiber optic ESPI. One way to achieve this is to wrap the reference beam fiber around a piezoelectric (PZT) cylinder such that an applied voltage to the PZT causes it to change dimensions and stretch the fiber producing a concomitant change in the phase of the interferometer. An alternative technique that we employed for a number of signal processing schemes was to modulate the emission frequency of a laser diode [36–40]. Combining this technique with an optical path length imbalance within the interferometer results in a concomitant change in the interferometer phase when the laser wavelength is changed. This approach is attractive as it removes

the requirement for any electrical components in the interferometer. Figure 20 shows the time-average vibration fringes obtained from the same gas turbine blade vibrating at 5.6 kHz. The bright white area of the fringes is where the surface of the blade is stationary, i.e. a nodal region.

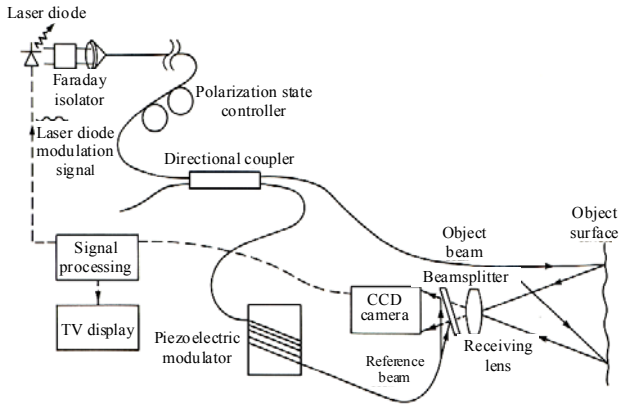

Fig. 18 Experimental arrangement for out-of-plane sensitive ESPI implemented using singlemode optical fiber and a laser diode source [36–40].

Fig. 19 Left–speckle image; middle and right–contour fringes of a gas turbine compressor blade: 190 GHz optical frequency modulation giving 0.9 mm fringes (middle) and 18.4 GHz optical frequency modulation giving 8 mm fringes (right).

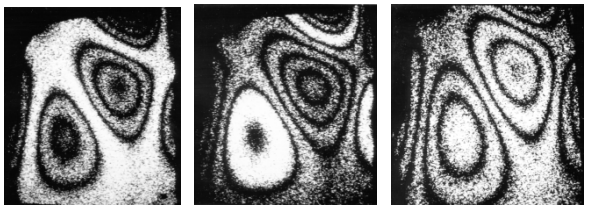

Fig. 20 Time-average (Bessel) correlation fringes from a gas turbine blade: vibrating at 5.6 kHz (Left–no heterodyning; middle–heterodyned by modulating the laser diode emission wavelength by 0.9 GHz with a path length imbalance of 1.15 m; right–stroboscopic illumination used pulsed laser diode generating cosine squared correlation fringes).

The amplitude and phase of the vibration pattern can be mapped out by modulating the phase of the interferometer, using either the fiber wound PZT or laser diode wavelength modulation, at the same frequency as the blade but with varying amplitude and phase, a technique called heterodyning.

Figure 20 shows the blade vibrating at 5.6 kHz but with the laser diode emission wavelength modulated by 0.9 GHz which, combined with an optical path length imbalance in the interferometer of 1.15 m, results in the area of the blade that is "effectively" stationary having moved to new positions. An alternative technique to recover phase information is to stroboscopically illuminate the vibrating surface, which can be readily achieved using a laser diode, which results in cosine squared fringes which can be then processed using phase shifting algorithms. Laser diodes can also be made to modulate between two distinct frequencies thus generating an effective wavelength much longer than the laser wavelength. This technique can be used to generate fringes on a test object that represent height contours which can be used to recover the shape of the object. This was one of the first areas of speckle I investigated, in collaboration with Prof. Julian Jones who had recently moved to Heriot-Watt University from the AOG, and the optics research group for Rover cars at Gaydon (UK) [39, 40]. Figure 19 shows contour fringes of a gas turbine compressor blade obtained by modulating the laser by 18 GHz–170 GHz [38, 39, 41].

We explored the potential of using low coherence techniques combined with ESPI for measuring object shapes [42]. A fiber network (Fig. 21), implemented in birefringent optical fiber is used to couple light from a broadband source to the object and to provide a reference beam that is obtained from a mirror mounted on the test object and, via a mirror mounted on a translation stage, used to adjust the depth position on the object at which measurements are made and combined with the light scattered from the test object on a CCD camera.

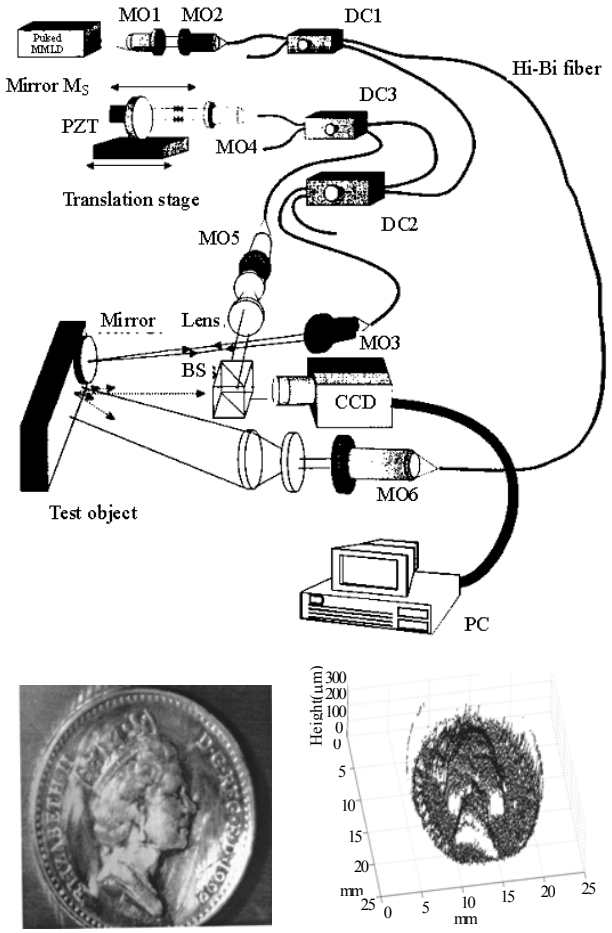

Fig. 21 Configuration for optical fiber-based low coherence speckle interferometry, with object-mounted reference mirror (MMLD: multimode laser diode; MO1–MO6: microscope objectives; DC1–DC3: polarization-maintaining directional couplers; PZT: piezoelectric mirror mount): the lower figures show a photo of a UK £1 coin and the surface relief of the coin obtained with the instrument).

A technique related to ESPI is speckle shearing interferometry, or shearography [43]. A typical arrangement is shown in Fig. 22. The output of a laser is expanded to illuminate the region of interest of the surface of the object under investigation. The scattered light forms a laser speckle pattern which is imaged through a Michelson shearing interferometer, onto a CCD camera. The shearing device serves to divide the image so that two identical, but displaced images are generated due to one of the mirrors being tilted, and images are recorded by the CCD camera. The two images combine coherently producing an interferometric speckle pattern at the sensor of the camera. In shearography the correlation fringes are sensitive to the displacement gradient rather than displacement as in ESPI. As such the fringe patterns are closely related to surface strain.

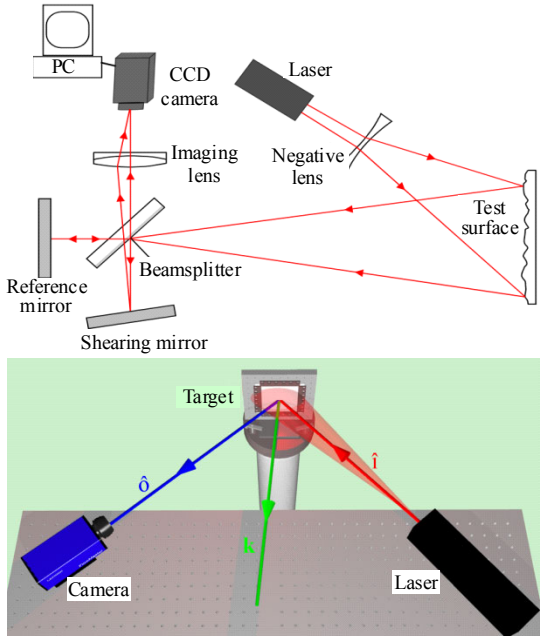

Fig. 22 A shearography system based on a Michelson shearing interferometer (the sensitivity vector, k, depends on the illumination, $\hat{\imath}$, and viewing direction, $\hat{o}$, lower figure, similar to the sensitivity vector discussed for Doppler velocimetry, and for near normal incidence and observation the system is sensitive to predominantly out-of-plane displacement gradients).

Shearography is inherently more resilient to environmental disturbances and vibrations than other ESPI because of its common path optical arrangement. As such it has become an important diagnostic tool, particularly in the field of non-destructive testing where it has been used primarily for qualitative inspection, for example, to reveal delaminations in composite structures such as aircraft tyres and aircraft skins. Our focus for shearography has been to explore the possibility of making the technique quantitative rather than just qualitative. Initially we investigated the use of modulated diode lasers to implement the phase stepping in an analogous manner to that described for ESPI. However, it is more complicated to introduce a path length imbalance into the

Michelson shearing interferometer and at the same time maintain the same image size for both images on the detector. We introduced a technique whereby a glass block [44] is placed in one arm of the shearing interferometer acting as a lens of zero power introducing a path length difference but maintaining the image size. Laser diode wavelength modulation was then used to implement phase shifting and heterodyning (Fig. 23) [45], and two-wavelength illumination from a diode laser for slope measurement [46]. We also reported a technique involving source displacement for shape and slope measurement [47].

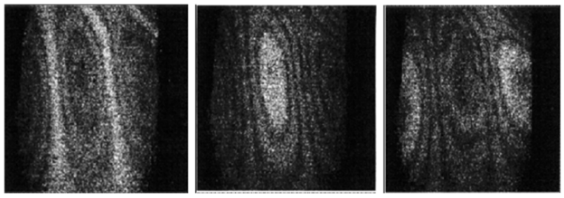

Fig. 23 Time averaged Bessel fringes from the same gas turbine as previously used vibrating at 5.6 kHz (heterodyned fringes with a relative phase shift of $\pi/2$ are shown in the middle and right figures).

A single observation and illumination direction based configuration measures only one displacement gradient component and therefore to get three components, the minimum needed to obtain quantitative surface strain, requires a minimum of either three illumination directions or three observation directions. Figure 24 shows an arrangement based on three illumination directions [48]. Each laser illuminates the test object sequentially. We implemented time-division-multiplexing using direct modulation of the laser diodes which was combined with the unbalanced Michelson interferometer described above to implement phase stepping. Figure 25 shows a photo of the current instrument using 50 mW frequency-doubled diode pumped YAG lasers and mechanical shutters. It is tripod mounted demonstrating its optically robust nature for field deployment. We developed a method based on shadow Moiré [49] to determine the source positions, important in precise determination of the surface strain, and investigated methods to implement phase unwrapping more efficiently, and therefore faster [50].

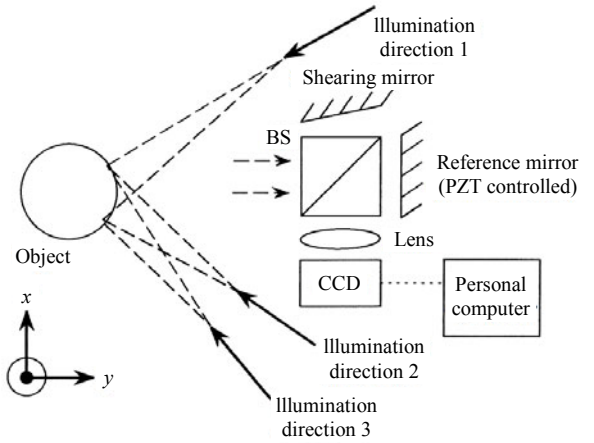

Fig. 24 Experimental layout for displacement gradient measurement (x, y represent directions in the plane and z out of the plane).

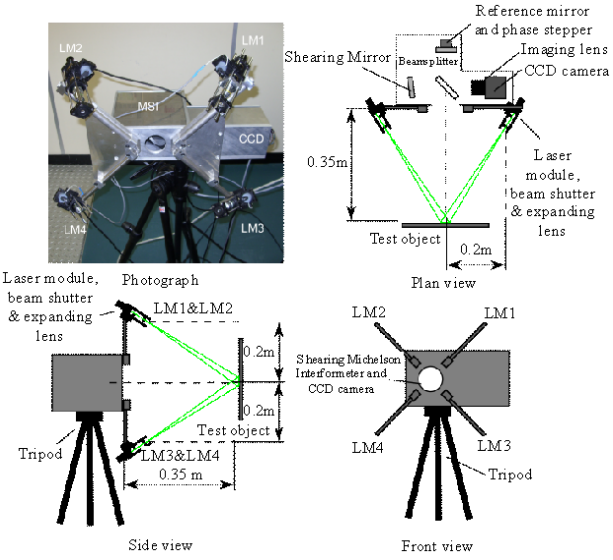

Fig. 25 Photo of quantitative shearography instrument with four illumination sources (LM1–LM4: laser modules).

Figure 26 shows the wrapped phase maps obtained using the experimental arrangement shown in Fig. 24 from the welded region of a pressure pipe, an area difficult or impossible to instrument using conventional techniques such as resistive foil strain gauges [51]. Each phase map is obtained from one

of the illumination directions shown in Fig. 24 for shear in the *x*-direction. Equivalent images are obtained for *y*-shear.

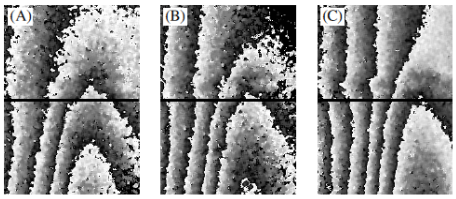

Fig. 26 Wrapped phase maps for a single shear direction for each of the 3 illumination directions (the field of view is 40 mm×55 mm, and the weld is horizontally across the center of the image, indicated by a black line).

Figure 27 shows the in-plane and out-of-plane quantitative displacement gradient maps calculated from the phase maps for the same region of the pipe [51]. This instrument was used to measure and characterize fatigue cracks in aerospace alloys and demonstrated that the technique had sufficient sensitivity to detect cracks even under protective coatings used on helicopter rotor heads [52]. We have shown that shearography can be combined with speckle photography to measure surface strain using a single illumination and viewing direction, useful for applications with restricted optical access [53].

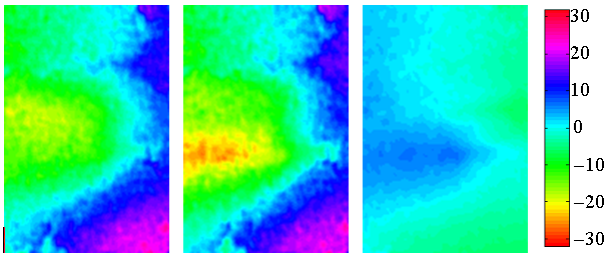

Fig. 27 In-plane and out-of-plane quantitative displacement gradient maps (the scale is in units of microstrain).

A technique to multiplex two shearing interferometers, for example configured to measure *x* shear and *y* shear respectively, and provide phase stepping without using any moving parts is shown in Fig. 28 [54]. A laser diode is coupled into birefringent optical fiber such that both eigenmodes are equally populated. Modulating the laser diode emission wavelength changes the SOP exiting the distal end of the optical fiber and illuminating the object. A polarizing beamsplitter is used to direct light to each shearing interferometer mirror, M_V and M_H, in turn as the laser wavelength changes. At the same time the laser wavelength modulation induces a phase shift in the interferometer phase using the glass block based path length imbalanced technique described earlier. Figure 29 shows how the injection current modulation, polarization state and phase within the interferometers are related.

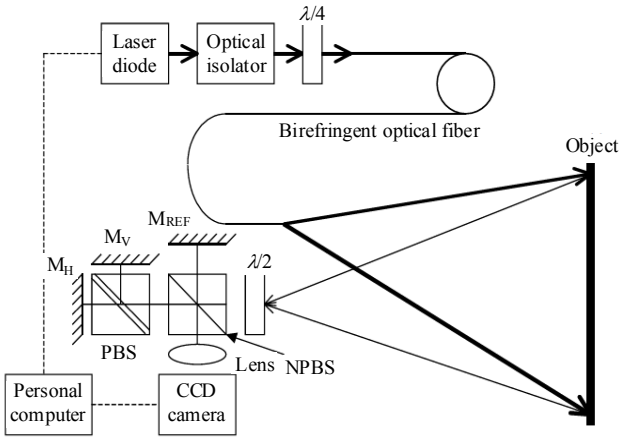

Fig. 28 Experimental layout of the polarization multiplexed shearography system: λ/4, quarter-wave plate; λ/2, half-wave plate; NPBS, non-polarizing beamsplitter cube; PBS, polarizing beamsplitter cube; M_{REF}, reference mirror; M_H and M_V, horizontal and vertical shearing mirrors respectively.

More recently we have incorporated the imaging fiber bundles described in Section 3.1 to implement an instrument based on multiple observation directions and used this with continuous wave [55] and pulsed [56] laser illumination, which could not have been fiber delivered due to the high peak energies produced by short pulsed lasers, to measure dynamic strain events.

Three viewing directions are the minimum required to measure quantitatively the full surface strain, however four separate measurement channels provide redundancy, particularly if one view is obscured due to object shape and, as we have shown recently [57], the fourth channel reduces the error in the calculated surface strain. Figure 30 shows a 3D rendering of the shearography instrumentation using

coherent imaging fiber bundles to provide four measurement channels and the instrument deployed on a mechanical test machine.

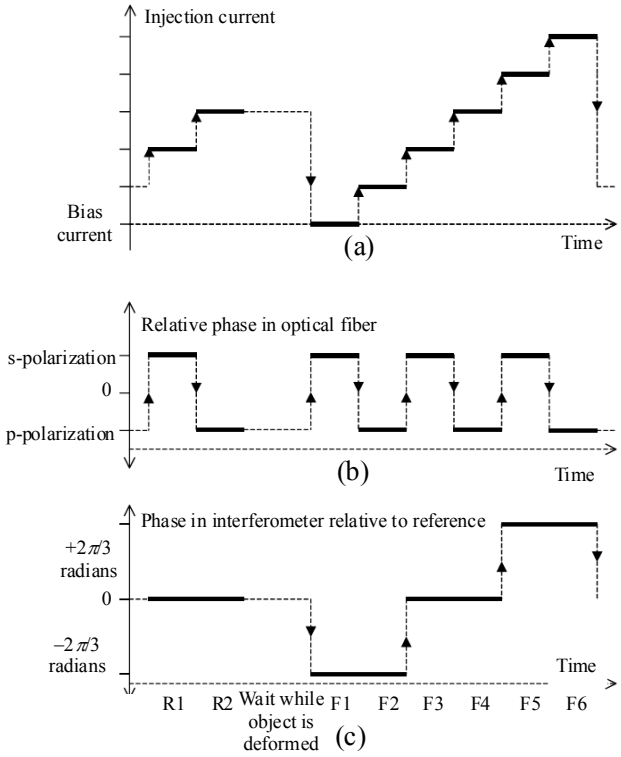

Fig. 29 (a) Laser diode injection current vs time relationship for a sequence of eight images (the injection current step is 4.025 mA), (b) relative phase in the optical fiber between the two orthogonal normal modes against time, and (c) relative phase in the interferometer between the image and the reference image with the same polarization against time (the polarization is s for frames R1, F1, F3 and F5 and p for frames R2 , F2 , F4 and F6).

In a current program we are investigating the use of speckle correlation techniques for high accuracy odometry on autonomous vehicles such as robots and rovers, and in particular for potential use with the interplanetary exploration rovers such as the ExoMars rover. Speckle velocimetry is intended to replace or supplement current odometry information provided by wheel encoders. A laser is used to produce a speckle pattern from the surface over which the rover travels and a CCD camera collects the scattered light. We have identified a normalized cross-correlation algorithm on sequential image frames as the most promising approach and have achieved odometry errors of 0.2% at speeds up to 1 mm/s. We expect the technique should scale well to higher velocities, about 85 mm/s, typical of exploration rovers [58].

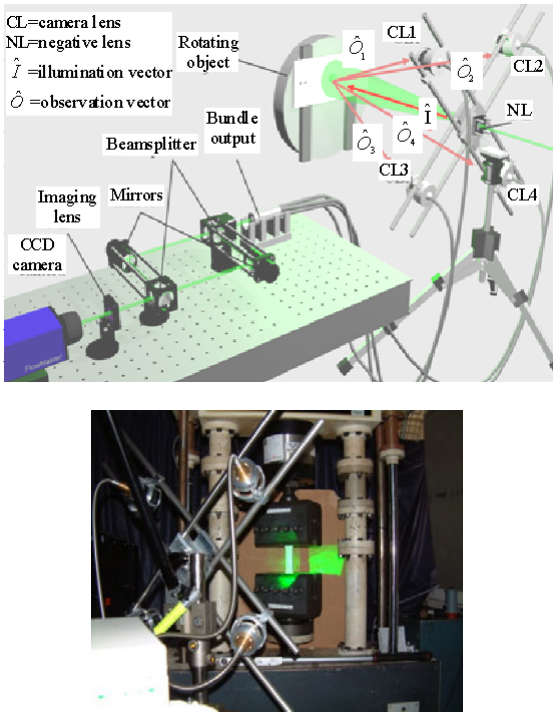

Fig. 30 Multi-component speckle shearography using imaging fiber bundles to measure full surface strain on a rotating object (top) (the arrows indicate the different sesnitivity vectors for each view and multi-component shearography instrument deployed on a mechanical test machine for dynamic measurements (bottom).

3.3 Optical gas sensors

More recently I have become involved with the development of optical instrumentation for gas sensing applications. This is an area of increasing importance with applications in health and safety, industrial process control, emissions monitoring and healthcare.

We are investigating non-dispersive infrared (NDIR) techniques for the measurement of CO_2 [59] and formaldehyde and high resolution spectroscopy based on tuneable diode laser absorption spectroscopy (TDLAS) techniques to detect a range of gases including methane [60–64]. A thrust of this research has been to improve the sensitivity by reducing the interference effects that occur from

using narrow linewidth lasers. This has included assessing the effects of self-mixing interference from specular and diffuse reflections within the instrument [61] and investigating gas cell designs using diffuse reflectors [62] and integrating spheres [63, 64], an example is shown in Fig. 31, and the issues associated with speckle that are introduced.

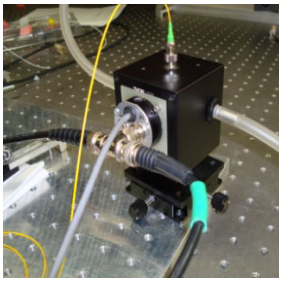

Fig. 31 Photo of an integrating sphere used with TDLAS for methane detection (the sphere is contained in a box of approximate dimensions 6 cm^3 and laser light is delivered by optical fiber to the top of the box and plastic pipes take gas in and out of the sphere.

Aspects of this TDLAS technology have now been commercialized for measuring methane in landfill applications [65].

3.4 Optical coherence tomography

My interest in optical coherence tomography (OCT) was initially in looking at techniques to overcome the problems with so called time-domain systems that used an optical fiber Michelson interferometer as the basis for the design. The issues were related to signal fading and noise due to differential polarization state and phase changes between the two interferometer arms. The arrangement we investigated was based on a fiber optic Fizeau sensing interferometer and a Michelson or Mach-Zehnder receiving/processing interferometer [66–69]. This configuration has the advantage of downlead insensitivity but at the cost of reduced overall S/N ratio due to the use of a receiving interferometer. The other issue we pursued was that of making an instrument capable of 3D operation but without any moving parts at the distal end of the probe, i.e. removing the requirement for electrical connections and moving components. To this end we have investigated the use of coherent imaging fiber bundles instead of a single optical fiber in the probe. Initially, all the fibers in the bundle were illuminated simultaneously with a low coherence source and a CCD camera was used as the detector [70] (Fig. 32). In this configuration many thousands of Fizeau interferometers are simultaneously addressed and parallel processed with a Michelson receiving interferometer. The configuration is downlead insensitive so that environmental perturbations on the imaging fiber bundle do not cause concomitant fluctuations in the interferometric signals. Both depth-slice and en-face imaging were demonstrated with this arrangement. The fiber bundle used here was of a leached construction containing over 5000 individual fiber cores of 8-μm core diameter on 10.6-μm centers (Fig. 33). Although crosstalk occurs between neighbouring fibers, this can be minimized with careful design [71]. Recently we have developed a swept source OCT system, and example images are shown in Fig. 34 for the system configured using a singlemode optical fiber, which utilizes an imaging fiber bundle, where the input optical beam is swept across the proximal face of the fiber bundle using either galvo scanners or an MEMS based scanning device [72] (Fig. 35).

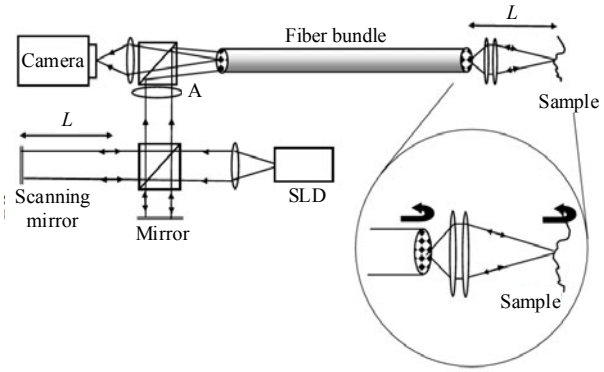

Fig. 32 Configuration for 3D time-domain common path OCT employing a fiber imaging bundle and CCD camera: SLD, super-luminescent diode at 830 nm and a 15-nm bandwidth; A, lens (the average path-length imbalance L is identical in both the Fizeau and Michelson interferometers,and the inset circle shows where the two reflections occur in the Fizeau interferometer).

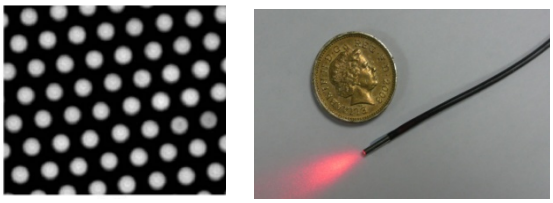

Fig. 33 Leached fiber bundle used in OCT instrumentation: CCD image of fiber end face, showing hexagonal packing arrangement with core diameters of 8 μm and core center spacing of 10.6 μm; flexible leached fiber bundle, showing guiding light from a He-Ne laser (Ferrule diameter is about 1 mm, shown with a UK £1 coin for comparison).

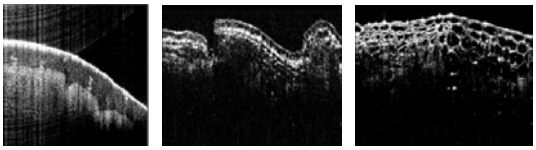

Fig. 34 Swept source OCT images using a laser centered at about 1300 nm with a 100-nm bandwidth (left – fingertip, showing sweat glands; middle and right – onions [73], demonstrating resolution at cellular level).

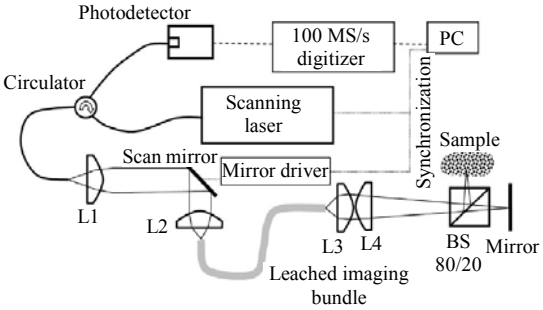

Fig. 35 Swept-source common path OCT incorporating a coherent fiber bundle with a miniature Michelson interferometer formed at the bundle output (L1–L4, lenses; BS, beamsplitter).

3.5 Optical fiber sensors

Early after my arrival at Cranfield I started to look at a number of signal processing techniques for use with a range of optical fiber sensors. One of the first was the use of stimulated Brillouin scattering (SBS) generated in optical fibers as a mechanism for an in-fiber frequency shifter. SBS is a nonlinear optical effect associated with the interaction of a pump signal, optically induced acoustic phonons, via electrostriction, and a frequency downshifted backscattered wave. The SBS frequency shift is in the range of 10 GHz–35 GHz for pump wavelengths of 1.5 μm–0.5 μm respectively. This frequency is generally too high for electronic signal processing and various techniques were investigated to reduce this to 10–100s MHz, for example, by mixing SBS signals generated from two separate reels of fiber at different temperatures. We investigated the potential of using birefringent optical fiber where SBS was generated in each polarization eigenmode at a slightly different frequency due to the difference in refractive index. Our initial research was focused on long lengths (800 m) of birefringent optical fiber pumped with several hundred milliwatts from a single frequency argon-ion laser emitting at 514.5 nm, for which the SBS frequency shift is about 34 GHz in silica fiber. The difference frequency between the eigenaxes, which is inversely proportional to the fiber beat length, was about 11 MHz for fiber with a 1-mm beatlength [74, 75]. To reduce the length of fiber and the pump power required we investigated the use of a fiber ring resonator fabricated from birefringent optical fiber [76]. At resonance the optical power coupled into the ring circulated many times producing gain (Fig. 36). For our experiments a 15-m ring made of Fujikura Panda fiber with a finesse of about 125 produced SBS for only a few microwatts of coupled power and a beat frequency of 11.7 MHz (Fig. 37). The temperature dependence of the beat frequency was measured to be (6.7 ± 0.5) kHz·K^{-1}.

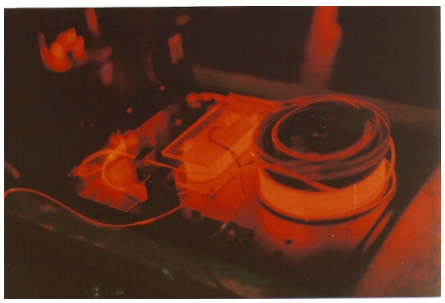

Fig. 36 Photo of a 15-m fiber optic ring resonator at resonance pumped with about 1 mW of light from a He-Ne laser operating at 632.8 nm.

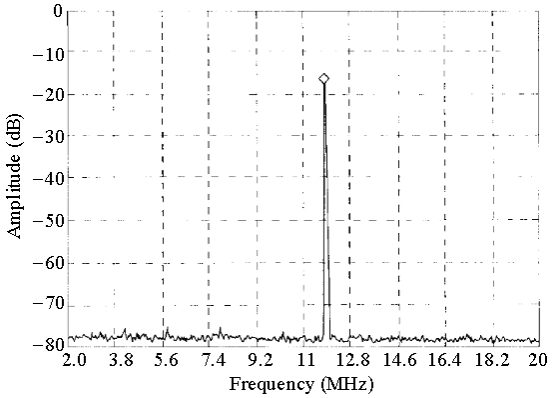

Fig. 37 Heterodyne beat frequency from birefringent optical fiber ring resonator pumped with a single frequency He-Ne laser at 632.8 nm (the peak is at 11.68 MHz and the resolution bandwidth is 100 kHz).

Another important area in the late 1980s/early 1990s was that of fiber optic components such as wavelength filters, before the general availability of the in-fiber Bragg grating (FBG). Continuing the theme of using birefringent optical fiber we explored the potential to make polarization based in-fiber components based on Solc filters [77]. The devices were made from a continuous length (<1m) of birefringent optical fiber of beatlength about 1 cm with several straight sections separated by twisted fiber sections to avoid cutting and splicing. The bandwidth depended on the number of sections but a four-section device demonstrated a bandwidth of 10 nm at 780 nm. We also demonstrated that polarization based multiplexing could be achieved using highly linearly birefringent (Hi-Bi) fiber and polarization selective fiber couplers [78].

Whilst investigating techniques for the interrogation of small Fabry-Perot cavities we realized that phase stepping techniques used in our speckle interferometry programs could be adapted and combined with multiwavelength sources to provide a passive method to recover the phase information from cavities with optical path differences of less than about 200 μm [79–82]. We exploited the characteristics of multimode laser diodes to lase on many individual modes to generate a multiwavelength source of equispaced wavelengths. The Fabry-Perot cavity interrogated was adjusted in size such that each wavelength provided an interferometric output with a relative phase difference of about $\pi/2$. The individual wavelengths were separated by a monochromator and detected by a CCD camera. Initially we used two wavelengths [79] but found that by moving to five wavelengths, and therefore five phase outputs, the phase errors arising from multiple reflections were reduced by two orders of magnitude. In addition, errors arising from mis-calibration of the cavity were also reduced by two orders of magnitude.

Shortly after my arrival at Cranfield I was introduced to Prof. Geoff Ashwell, a chemist at Cranfield. We went on to collaborate successfully for many years until his retirement earlier this year. Geoff worked for many years on designing and synthesizing organic materials for non-linear optics applications and characterized his materials by depositing them at the molecular scale on microscope slides using the Langmuir-Blodgett (LB) technique; this is a method that allows room temperature deposition without a vacuum of films a single molecule thick onto substrates, and for thick films to be built up by depositing many individual layers each of which is 1 nm–3 nm thick. My interest was to take this technique and to adapt it use optical fibers as the substrate as this would allow a new class of fiber device for signal processing, sensing and non-linear optics applications.

Our initial efforts were targeted at being able to deposit the films onto singlemode optical fiber with the cladding polished away to reveal the core to form an overlay waveguide device (Fig. 38). This led to us learning how to lap and polish optical fibers, initially with the fibers glued in grooves in glass blocks [83] and subsequently using a freely suspended optical fiber polishing technique which required no substrate or epoxy and allowed more repeatable LB deposition [84]. We demonstrated that LB films could be deposited successfully onto optical fibers using both these methods and that the

precise control over the film thickness to about 3 nm was vital in achieving the optimum coating thickness. Films of ω-tricosenoic acid were used to form channel dropping filters (Fig. 39), and a merocyanine dye was used as a pH and chemical sensor [85, 86]. Subsequently we developed a technique to allow non-centrosymmetric deposition of the films onto an optical fiber [87, 88] and demonstrated that this could be used for second harmonic generation by coupling a pump laser into the fiber and employing Cerenkov phase matching at the waveguide overlay [89] (Fig. 40). We further modified the LB deposition technique to form sub-micron cavities on the ends of optical fibers for sensing applications [90].

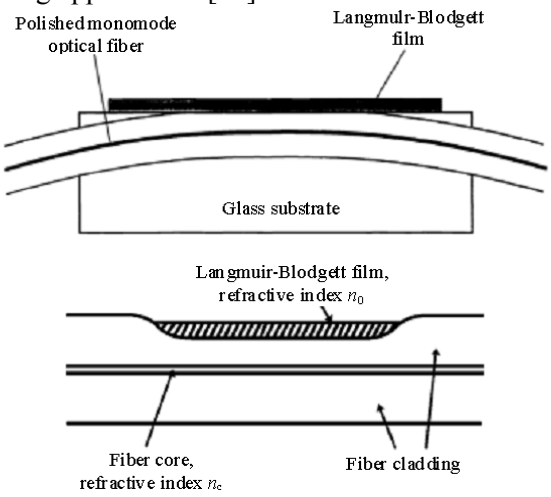

Fig. 38 Schematic of fiber glued in groove in glass block (left) and freely suspended (right).

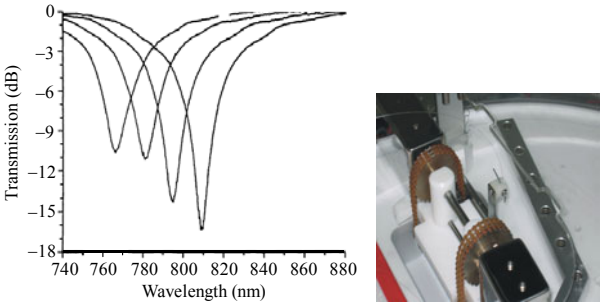

Fig. 39 Channel dropping filter response of ω-tricosenoic acid deposited onto a side polished optical fiber (from left to right 112-114-116-118 bilayers demonstrating the precise film thickness control required to optimize the performance of the device) and photo showing modified LB trough dipping mechanism for depositing molecular films onto optical fibers.

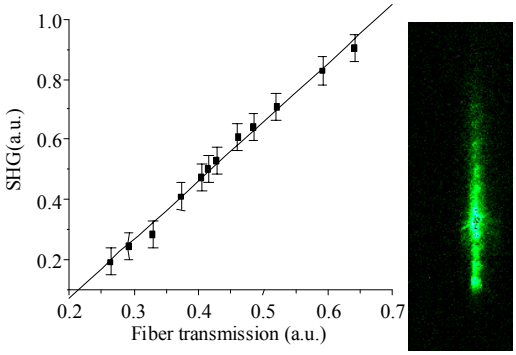

Fig. 40 SHG vs fiber coupled optical power at 21.4 ℃ (1.064-μm pump laser) showing expected dependence (photo of Cerenkov phase matched SHG emitted from the side of the optical fiber measured with a CCD camera).

With the advent of the in-fiber Bragg grating I concluded in the early 1990's that we should invest in our own fabrication facility as many of the applications we envisaged required custom grating wavelengths or arrays that were commercially unavailable and not easy to obtain from other laboratories at the time. The laser we chose also had to be capable of being used for other programs such as the flow measurement and speckle metrology discussed previously. The system employed an injection-seeded frequency-doubled YAG laser that pumped a dye laser. The output from the dye laser was frequency-doubled and sum-frequency mixed with residual infrared light to give a tuneable wavelength output from 240 nm–265 nm (Fig. 41). We used the wavelength tuneability of this source combined with a phase mask based interferometer arrangement to write FBGs [91] with high resolution control over the FBG center wavelength and have used it to fabricate gratings with central wavelengths from 500 nm to 1650 nm.

We explored several signal processing techniques for interrogating FBG sensor arrays [92–96] including a technique based on photorefractive volume holographic technique [92]. In this approach an FBG sensor is interrogated using a matched holographic grating filter. We demonstrated this with a photorefractive crystal, although other holographic recording media would

also be useable. The potential advantage is that many hundreds of receiving gratings can be written into a single holographic element providing a very compact and high speed interrogation system; the electrical bandwidth only depends on that of the detectors used. We have also used FBGs to provide controlled feedback into Fabry-Perot lasers operating at wavelengths from 650 nm–850 nm to control the emission wavelength. This was used for example, to stabilize the laser output for applications in laser anemometry and speckle interferometry [24, 51] and to provide tuneable and multiwavelength outputs for sensing applications [97]. In the later example [97], gratings were written in Hi-Bi fiber to exploit the intrinsic birefringence to generate two FBGs separated in wavelength by 0.3 nm for fiber with a beatlength of 1.6 mm. The wavelength separation was tuned by applying transverse load to the fiber at the location of the FBGs.

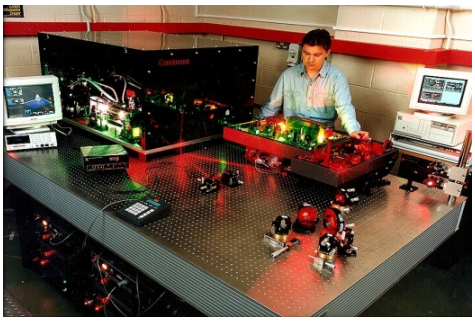

Fig. 41 Our first laser system used for FBG fabrication that is still used extensively: njection-seeded, frequency-doubled YAG laser pumping a dye laser [output from the dye laser is frequency-doubled and sum-frequency-mixed with residual infrared (IR) light to generate tuneable ultra violet (UV) light in 240 nm–265 nm range].

More recently the focus of our FBG research has been in applying them to industrial measurement problems. This led us to investigate the mechanical and thermal performance of FBGs to assess the influence of stripping the jacket and hydrogen loading in order to fabricate the FBG (Fig. 42), as well as issues associated with embedding the FBG sensors in composite materials and benchmarking their performance [98–104].

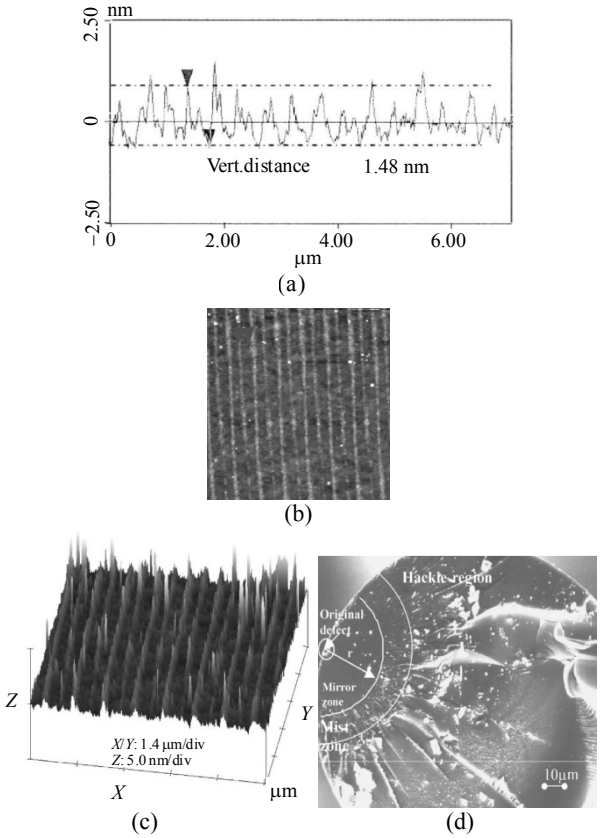

Fig. 42 Atomic force microscope image of UV-irradiated surface for Ge-B codoped fibers under 2.4 W/cm^2 from an injection-seeded frequency-quadrupled YAG laser emitting at 266 nm with a 10-Hz repetition rate and 5-ns pulse duration: (a) surface cross-section spectrum, (b) 2D surface image (7 μm×7 μm), (c) 3D surface image, and (d) fracture surface showing failure initiated from surface, a mirror zone, mist zone and hackle region in hydrogen loaded and UV irradiated fiber with a fracture stress of 603 MPa.

The application areas to which we have applied FBG sensors are extensive including, for example, sensors for cure and health and usage monitoring in composite materials for aerospace and cryogenic applications [105–111], structural monitoring [112], dynamic measurements on military gun barrels [113] (Fig. 43), geotechnical applications [114–116], aerodynamic pressure sensing [117] and rail monitoring [118]. For example, we undertook dynamic strain measurement on a 30-mm diameter gun barrel where the exit velocity of the shell was more than 1 km/s and demonstrated that FBG sensors were capable of monitoring transient strain

signatures of duration of less than 100 μs and magnitudes up to 10,000 μm/m [113]. The rationale for this work is to investigate FBG sensors, and the immunity to electromagnet fields that they offer, as replacements for resistive foil strain gauges which would not work in the harsh electromagnetic environment of guns based upon electromagnetic, electro-thermal or electro-chemical propulsion.

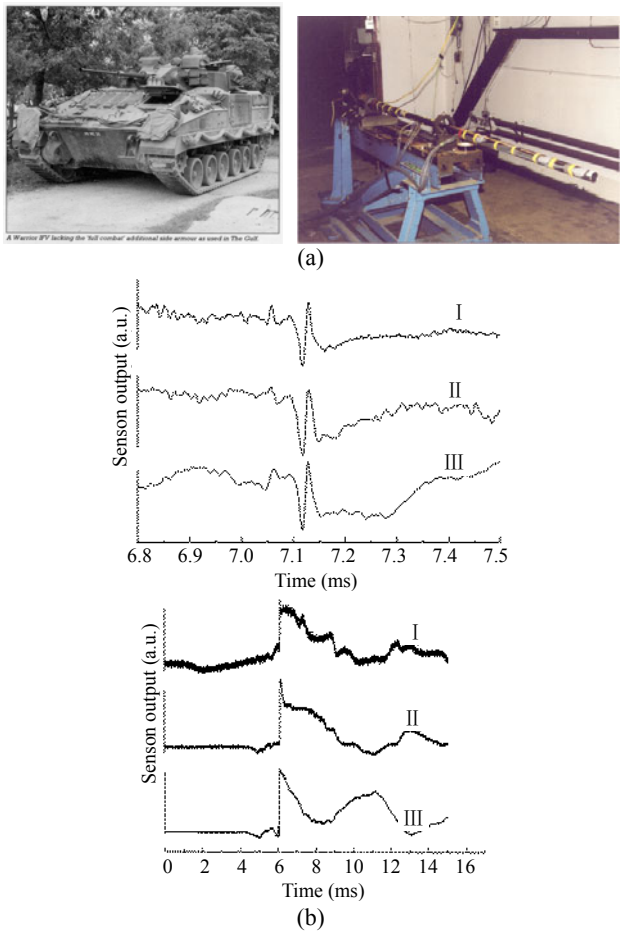

Fig. 43 (a) FBG sensors attached to 30-mm gun barrel from a "warrior" vehicle (exit velocity of 30-mm shell is about 1 km/s) and (b) axial (middle) and radial (bottom) strain responses: Ⅰ and Ⅱ FBG sensors and Ⅲ resistive foil strain gauge [113].

As part of our research on aerodynamic sensors we looked at new ways of measuring pressure based on applying a load to the central portion of an FBG such that it introduced a spectral hole in the FBG spectrum (Fig. 44). This spectral hole provided a high resolution mechanism to measure pressure and at the same time was temperature insensitive since temperature moved the central wavelength of the FBG spectrum but not the relative position of the spectral hole within the FBG envelope.

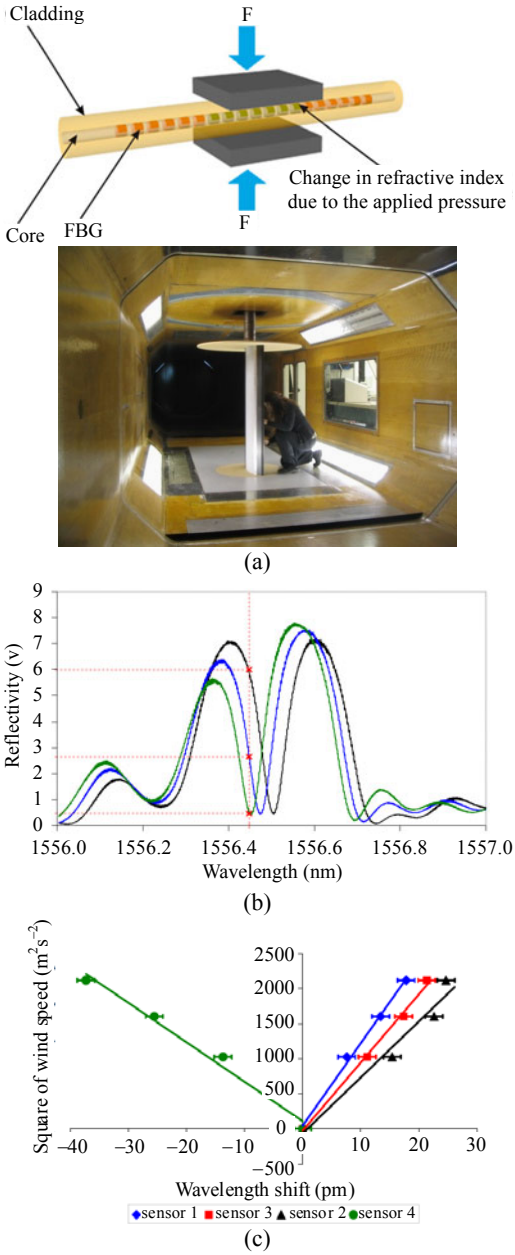

Fig. 44 (a) Pressure sensor based on a spectral hole generated by a transverse load applied to part of an FBG (photo of installation of FBGs mounted in an aerofoil test section in the 8'×6' windtunnel at Cranfield), (b) FBG spectrum showing spectral hole movement as a function pressure: curve at left, 0kPa; middle curve, 122kPa; right hand curve, 245kPa, and (c) windtunnel results for sensors on top and bottom surfaces of aerofoil.

We developed this approach further for load sensing [119–121] and for pore water pressure monitoring in geotechnical applications [122]. As part of our program of employing FBGs as sensors embedded within composite materials we investigated the potential of FBGs written in Hi-Bi fiber for the measurement of transverse strain in addition to longitudinal strain measurement. This involved developing new instrumentation [123, 124] and a detailed characterization of Hi-Bi fiber properties [125].

This proved effective at measuring the onset of gelation in the cure process [106] and was subsequently used to measure stress in superconducting magnets during energisation and quench [111], i.e., when the magnet coil changed from superconducting to non-superconducting in a short timeframe imposing stress on the structure (Figs. 45 and 46). Conventional sensors are unable to operate at the temperatures found in cryogenic systems, and fiber sensors are able to offer new insight into the designers.

In the area of geotechnical engineering we have been applying FBG sensors to the monitoring of pile loading tests at sites in Hull and Wembley. The FBG sensors have been installed on different designs of piles and used in static and dynamic testing and have demonstrated their potential in this application area [116] (Fig. 47).

Fig. 45 FBG sensors deployed in superconducting magnets.

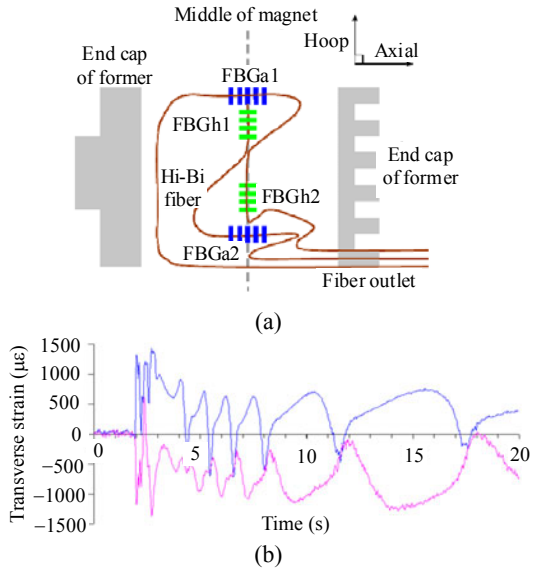

Fig. 46 (a) Schematic of FBG layout on a horizontal magnet as shown in Fig. 45, lower left and (b) transverse strain measured by Hi-Bi fiber embedded in composite coil in superconducting magnet during quench for hoop (top trace) and axial (bottom trace) orientated Hi-Bi FBGs.

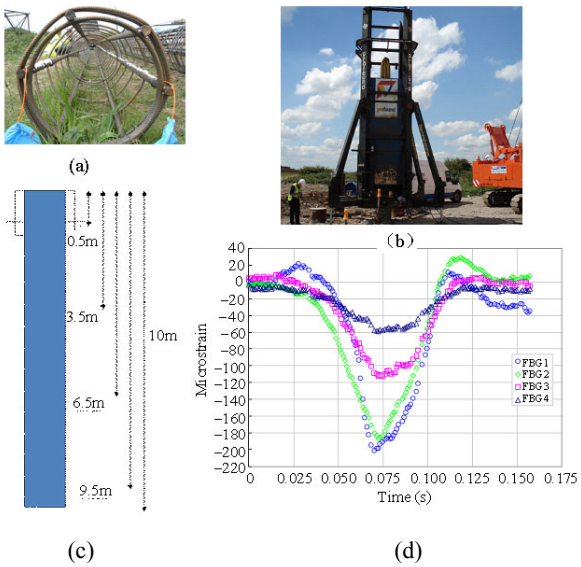

Fig. 47 (a) FGB instrumented reinforcement cage, (b) statnamic testing, (c) schematic showing location of FBG sensors along 10 m of cage, and (d) strain vs time calculated from FBG wavelength shifts.

Long period fiber gratings (LPGs) are also an area of active research within my laboratories. These devices couple core modes to cladding modes and are therefore sensitive to materials surrounding the optical fiber. Our initial investigations were aimed at

characterizing the devices [126–130], investigating signal processing techniques [131] and more recently depositing nanoscale films, using the LB and other self-assembly techniques, around the LPG for chemical and gas sensing applications [132–138]. An interesting outcome has been to demonstrate experimentally that the dual resonant bands (Fig. 48), that occur near the phase matching turning point can be exploited to increase the sensitivity of devices, for example, we observed a sensitivity of 1.45 nm/nm for the shift in the wavelength of the band per nm of coating deposited. To achieve this requires precise control of the thickness of the overlay deposited, provided by the LB technique, and modelling of the dispersion curves of the LPG with the overlay. Recently we have been investigating tapered optical fibers [139] (Fig. 49), as a means of accessing the evanescent field for chemical and gas sensing and combining the tapers with grating technology for high sensitivity sensing.

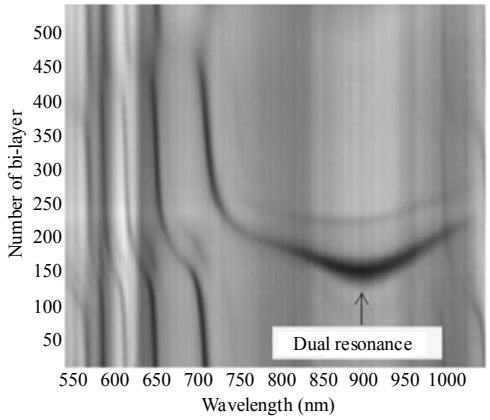

Fig. 48 Grey scale plot illustrating the response of the transmission spectrum of an LPG of period 180 μm to the deposition of a coating of calix-4-resorcarene using the LB technique (the spectra were recorded with the LPG in the air subphase, and the attenuation band originating at approximately 900 nm shows the development of the dual resonance effect).

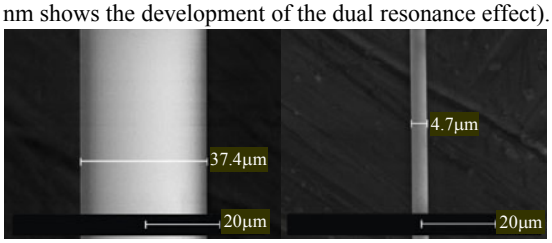

Fig. 49 Environmental scanning electron microscope images of tapered fiber waists produced using a flame.

4. Summary

This paper has provided me with the opportunity to present a short overview of my research at the University of Kent whilst I was a member of the Applied Optics Group followed by a summary of my research interests since I have been at Cranfield.

Acknowledgment

I would like to thank all my colleagues during my time that I was a member of the AOG both for their help and guidance and also for making it an enjoyable group in which to work, and to David Jackson in particular for his inspirational leadership. I would also like to take this opportunity to thank all the members of my own research team whom I have been privileged to lead over the last 22 years. There is not space to name everyone individually as there have been more than 50 PhD students and almost 25 members of staff during this time but several people have been in the team for many years and have made many significant contributions. These include, in order of longevity within the team, Helen Ford, Steve Staines, Steve James, Edmon Chehura, Tom Charrett, and Jane Hodgkinson. Many thanks to the many research collaborators with whom it has been both an education and a pleasure to work over the years and finally, to the many organizations who have sponsored my research during this time, including: SERC/EPSRC (UK) and PPARC (UK), the Royal Society (UK), Higher Education Funding Council for England, the European Union, the Technology Strategy Board, Advantica, AEA Technology, Airbus, Alphasense, Alstom Gas Turbines, AOS, Agusta Westland Helicopters, AWE, BAE Systems, BTG, CAA, DRA, EADS Astrium, Elster, ERA Technology, Geotechnical Instruments, Gloucester Royal Hospital, GKN, Oxford Instruments, Protolog, Rolls-Royce, Rover Group, Siemens, Siemens Cerberus.

References

[1] R. P. Tatam, J. D. C. Jones, and D. A. Jackson, "Optical polarization state control schemes using fiber optics or Bragg cells," *J. Phys. E: Sci. Instrum.*, vol. 19, no. 9, pp. 711–717, 1986.

[2] R. P. Tatam, J. D. C. Jones, and D. A. Jackson, "Opto-electronic processing schemes for the measurement of circular birefringence," *Optica Acta*, vol. 33, no. 12, pp. 1519–1528, 1986.

[3] C. N. Pannell, R. P. Tatam, J. D. C. Jones, and D. A. Jackson, "Two-dimensional fiber optic laser velocimetry using polarization state control," *J. Phys. E.: Sci. Instrum.*, vol. 21, no. 1, pp. 103–107, 1988.

[4] R. P. Tatam, M. Berwick, J. D. C. Jones, and D. A. Jackson, "Faraday effect magnetometry utilizing high Verdet constant glass," *Appl. Phys. Lett*., vol. 51, no. 11, pp. 864–866, 1987.

[5] R. P. Tatam, D. C. Hill, J. D. C. Jones, and D. A. Jackson, "All-fiber optic polarization state azimuth control: application to Faraday rotation," *J. Lightwave Technol.*, vol. 6, no. 7, pp. 1171–1176, 1988.

[6] R. P. Tatam and D. A. Jackson, "Remote probe configuration for Faraday effect magnetometry," *Opt. Commun.*, vol. 72, no. 1, 2, pp. 60–65, 1989.

[7]R. P. Tatam, M. Berwick, P. Akhavan Leilabady, J. D. C. Jones, and D. A. Jackson, "Applications of Faraday rotation using monomode optical fiber," in *Proc. SPIE*, vol. 734, pp. 178–192, 1987.

[8] A. P. Steer, S. J. Turner, P. R. B. Farrie, D. King, A. N. Tobin, R. P. Tatam, J. D. C. Jones, and D. A. Jackson, "Application of an optical fiber current sensor to electricity supply protection," in *Proc. SPIE*, vol. 1120, pp. 324–331, 1989.

[9] R. P. Tatam, C. N. Pannell, J. D. C. Jones, and D. A. Jackson, "Full polarization state control utilizing linearly birefringent monomode optical fiber," *J. Lightwave Technol.*, vol. LT-5, no. 7, pp. 980–985, 1987.

[10] C. N. Pannell, R. P. Tatam, J. D. C. Jones, and D. A. Jackson, "Optical frequency shifter using linearly birefringent monomode Fiber," *Electron. Lett.*, vol. 23, no. 16, pp. 847–848, 1987.

[11] C. N. Pannell, R. P. Tatam, J. D. C. Jones, and D. A. Jackson, "A fiber optic frequency shifter utilizing travelling flexure waves in birefringent fiber," *J. IERE*, vol. 58, no 5, pp. S92–S98, 1988.

[12] S. R. Waite, R. P. Tatam, and D. A. Jackson, "Use of optical fiber for damage and strain detection in composite materials," *Composites*, vol. 19, no. 6, pp. 435–442, 1988.

[13] D. J. Webb, R. P. Tatam, and D. A. Jackson, "A novel interferometric liquid refractometer," *Rev. Sci. Instrum.*, vol. 60, no. 10, pp. 3347–3348, 1989.

[14] D. J. Webb, R. P. Tatam, J. D. C. Jones, and D. A. Jackson, "A novel technique for polarization mode dispersion measurements in optical fibers," *Opt. Commun.*, vol. 69, no. 3/4, pp. 230–234, 1989.

[15] P. Merritt, R. P. Tatam, and D. A. Jackson, "Interferometric chromatic dispersion measurements on short lengths of monomode optical fiber," *J. Lightwave Technol.*, vol. 7, no. 4, pp. 703–716, 1989.

[16] ISI Web of Science (wok.mimas.ac.uk*)*, Accessed April 2011.

[17] R. P. Tatam, G. Rollinson, J. D. C. Jones, and D. A. Jackson, "High resolution optical fiber thermometer: applications to biotechnology," *Biotechnology Techniques*, vol. 1, no. 1, pp. 11–14, 1987.

[18] S. W. James, R. P. Tatam, and R. L. Elder, "Design considerations for a 3D fiber optic laser Doppler velocimeter for turbomachinery applications," *Rev. Sci. Instrum.*, vol. 68, no. 8, pp. 3241–3246, 1997.

[19] S. W. James, R. A. Lockey, D. A. Egan, and R. P. Tatam, "Fiber optic based reference beam laser Doppler velocimeter," *Opt. Commun.*, vol. 119, no. 5–6, pp. 460–464, 1995.

[20] G. D. Byrne, S. W. James, and R. P. Tatam, "A single-headed fiber optic laser Doppler anemometer probe for the measurement of flow angles," *Meas. Sci. Instrum.*, vol. 15, no. 1, pp. 1–8, 2004.

[21] E. Chehura and R. P. Tatam, "In-line laser Doppler velocimetry using fiber optic Bragg grating interferometric filters," *Meas. Sci. Technol.*, vol. 14, no.6, pp. 724–735, 2003.

[22] D. Egan, S. W. James, and R. P. Tatam, "On-axis laser Doppler velocimeter for turbomachinery applications using optical fiber techniques," in *Proc. SPIE*, vol. 3172, pp. 17–26, 1997.

[23] D. A. Egan, S. W. James, and R. P. Tatam, "A polarization-based optical fiber vibrometer," *Meas. Sci. Technol.*, vol. 8, no. 3, pp. 343–347, 1997.

[24] G. D. Byrne, S. W. James, and R. P. Tatam, "A Bragg grating based fiber optic reference beam laser Doppler anemometer," *Meas. Sci. Instrum.*, vol. 12, no. 7, pp. 909–913, 2001.

[25] R. A. Lockey and R. P. Tatam, "Multi-component time-division multiplexed optical fiber laser Doppler anemometry," *IEE Proc. Optoelec.*, vol. 144, no. 3, pp. 168–175, 1997.

[26] H. D. Ford and R. P. Tatam, "Development of extended field Doppler velocimetry for turbomachinery applications," *Opt. Lasers. Eng.*, vol. 27, no. 6, pp. 675–696, 1997.

[27] D. S. Nobes, H. D. Ford, and R. P. Tatam, "Instantaneous, three-component planar Doppler velocimetry using imaging fiber bundles," *Expt. Fluids*, vol. 36, no. 1, pp. 3–10, 2004.
[28] D. S. Nobes, B. Weinke, and R. P. Tatam, "Determination of view vectors from image warping mapping functions," *Opt. Eng.*, vol. 43, no. 2, pp. 407–414, 2004.
[29] T. O. H. Charrett, H. D. Ford, D. S. Nobes, and R. P. Tatam, "Two-frequency planar Doppler velocimetry," *Rev. Sci. Instrum*., vol. 75, no. 11, pp. 4487–4496, 2004.
[30] T. O. H. Charrett and R. P. Tatam, "Investigation into the selection of viewing configurations for 3D planar Doppler velocimetry (PDV) techniques," *Appl. Opt.*, vol. 46, no. 19, pp. 4102–4116, 2007.
[31] Z. H. Lu, T. O. H. Charrett, H. D. Ford, and R. P. Tatam, "Mach-Zehnder interferometric filter based planar Doppler velocimetry (MZI-PDV)," *J. Opt. A.: Pure & Appl. Opt.*, vol. 9, no. 11, pp. 1002–1013, 2007.
[32] Z. H. Lu, T. O. H. Charrett, and R. P. Tatam, "Three-component planar velocity measurement using Mach-Zehnder interferometric filter based planar Doppler velocimetry," *Meas. Sci. Technol*., vol. 20, no. 3, pp. 034019 (15 pages), 2009.
[33] C. Willert, G. Stockhausen, M. Beversdorff, J. Klinner, C. Lempereur, P. Barricau, J. Quest, and U. Jansen, "Application of Doppler global velocimetry in cryogenic wind tunnels," *Expt. Fluids*, vol. 39, no. 2, pp. 420–430, 2005.
[34] J. F. Meyers, J. W. Lee, M. T. Fletcher, A. A. Cavone, and J. A. G. Viramontes, "Supersonic flow field investigations using a fiber-optic based Doppler global velocimeter," presented at *13th Int. Symp. on Applications of Laser Techniques to Fluid Mechanics (Paper 1019)*, Lisbon, Portugal, June 26–29, 2006.
[35] J. Potter and R. P. Tatam, "Optical condensation measurement in gas turbine engine inlets," in *Proc. SPIE*, vol. 3172, pp. 424–435, 1997.
[36] H. Atcha and R. P. Tatam, "Heterodyning of fiber optic electronic speckle pattern interferometers using laser diode wavelength modulation," *Meas. Sci. Technol.*, vol. 5, no. 6, pp. 704–709, 1994.
[37] A. Olszak and R. P. Tatam, "The calibration of the path-length imbalance in optical fiber ESPI systems employing source- wavelength modulation," *Meas. Sci. Technol.*, vol. 8, no. 7, pp. 759–763, 1997.
[38] H. D. Ford, H. Atcha, and R. P. Tatam, "Optical fiber technique for measurement of small frequency separations: application to surface profile measurement using electronic speckle pattern interferometry," *Meas. Sci. Technol.*, vol. 4, no. 5, pp. 601–607, 1993.
[39] R. P. Tatam, J. C. Davies C. H. Buckberry, and J. D. C. Jones, "Holographic surface contouring using wavelength modulation of laser diodes," *Opt. Las. Technol*., vol. 22, no. 5, pp. 317–321, 1990.
[40] H. Atcha, R. P. Tatam, C. H. Buckberry, J. C. Davies, and J. D. C. Jones, "Surface contouring using TV holography," in *Proc. SPIE*, vol. 1504, pp.221–232, 1991.
[41] R. P. Tatam, "Optical fiber speckle interferometry" in *Optical fiber sensor technology*, vol. 2 (Devices and technology). K. T. V. Grattan and B. T. Meggitt Ed. London: Chapman & Hall, 1998.
[42] I. Balboa, H. D. Ford, and R. P. Tatam, "Low-coherence optical fiber speckle interferometry," *Meas. Sci. Technol*., vol. 17, no. 4, pp. 605–616, 2006.
[43] D. Francis, R. P. Tatam, and R. M. Groves, "Shearography technology and applications: a review," *Meas. Sci. Technol*., vol. 21, no. 10, pp. 102001–102029, 2010.
[44] J. R. Huang, H. D. Ford, and R. P. Tatam "Phase-stepped speckle shearing interferometer by source wavelength modulation," *Opt. Lett*., vol. 21, no. 18, pp. 1421–1423, 1994.
[45] J. R. Huang, H. D. Ford, and R. P. Tatam, "Heterodyning of speckle shearing interferometers using laser diode wavelength modulation," *Meas. Sci. Technol.*, vol. 7, no. 12, pp. 1721–1727, 1996.
[46] J. R. Huang, H. D. Ford, and R. P. Tatam, "Slope measurement by two-wavelength electronic shearography," *Opt. Laser Eng.*, vol. 27, no. 3, pp. 321–333, 1997.
[47] R. M. Groves, S. W. James, and R. P. Tatam, "Shape and Slope measurement by source displacement in shearography," *Opt. Lasers Eng.*, vol. 41, no. 4, pp. 124–127, 2004.
[48] S. W. James and R. P. Tatam, "Time-division-multiplexed 3D shearography," in *Proc. SPIE*, vol. 3745, pp. 114–133, 1999.
[49] R. M. Groves, S. W. James, and R. P. Tatam, "Shadow Moiré method for the determination of the source position in three-dimensional shearography," *Opt. Lasers Eng*., vol. 36, no. 4, pp. 317–329, 2001.
[50] F. Sawaf and R. P. Tatam "Finding minimum spanning trees more efficiently for tile based phase unwrapping," *Meas. Sci. Technol*., vol. 17, no. 6, pp. 605–616, 2006.
[51] R. M. Groves, S. W. James, and R. P. Tatam, "Pipe weld investigation using shearography," *Strain*, vol. 39, no. 3, pp. 101–105, 2003.
[52] R. M. Groves, D. Furfari, S. E. Barnes, S. W. James, S. Fu, P. E. Irving, and R. P. Tatam, "Full-field laser shearography instrumentation for the detection and characterization of fatigue cracks in titanium 10-2-3," *J. ASTM International*, vol. 3, no. 4, pp. JAI-12757 (13 pages), 2006.
[53] R. M. Groves, S. Fu, S. W. James, and R. P. Tatam, "Single-axis combined shearography and digital speckle photography instrument for full surface

strain measurement," *Opt. Eng.*, vol. 44, no. 2, pp. 025602 (6 Pages), 2005.

[54] R. M. Groves, S. W. James, and R. P. Tatam, "Polarization multiplexed and phase-stepped fiber optic shearography using laser wavelength modulation," *Meas. Sci. Technol.*, vol. 11, no. 9, pp. 1389–1395, 2000.

[55] D. Francis, S. W. James, and R. P. Tatam, "Surface strain measurement using multi-component shearography with fiber optic imaging bundles," *Meas. Sci. Technol.*, vol. 18, no. 11, pp. 3583–3591, 2007.

[56] D. Francis, S. W. James, and R. P. Tatam, "Surface strain measurement of rotating objects using pulsed laser shearography with coherent fiber-optic imaging bundles," *Meas. Sci. Technol.*, vol. 19, no. 10, pp. 105301 (13 pages), 2008.

[57] T. O. H. Charrett, D. Francis, and R. P. Tatam, "Quantitative shearography: error reduction by using more than three measurement channels," *Appl. Opt*., vol. 50, no. 2, pp. 134–146, 2011.

[58] T. O. H. Charrett, L. Waugh, and R. P. Tatam, "Speckle velocimetry for high accuracy odometry for a Mars exploration rover," *Meas. Sci. Technol*., vol. 21, no. 2, pp. 125301 (12 pages), 2010.

[59] R. A. Zakaria, J. Hodgkinson, and R. P. Tatam, "Characterization of mid-IR sources and detectors for use in NDIR carbon dioxide gas sensing," presented at *Proc. Pittcon 2009 (Paper 3000-2)*, Chicago, March 8–13,**,** 2009.

[60] D. Masiyano, J. Hodgkinson, S. Schilt, and R. P. Tatam, "Self-mixing interference effects in tunable diode laser absorption spectroscopy," *Appl. Phys. B*, vol. 96, no. 4, pp. 863–874, 2009.

[61] D. Masiyano, J. Hodgkinson, and R. P. Tatam, "Use of diffuse reflections in tunable diode laser absorption spectroscopy: implications of laser speckle for gas absorption measurements," *Appl. Phys. B*, vol. 90, no. 2, pp. 279–288, 2008.

[62] J. Hodgkinson, D. Masiyano, and R. P. Tatam, "Gas cells for tunable diode laser absorption spectroscopy employing optical diffusers. part 1: single and dual pass cells," *Appl. Phys. B*, vol. 100, no. 2, pp. 291–302, 2010.

[63] D. Masiyano, J. Hodgkinson, and R. P. Tatam, "Gas cells for tunable diode laser absorption spectroscopy employing optical diffusers. part 2: integrating spheres," *Appl. Phys. B*, vol. 100*,* no. 2, pp. 303–312, 2010.

[64] J. Hodgkinson, D. Masiyano, and R. P. Tatam, "Using integrating spheres as absorption cells: pathlength distribution and application of Beer's law," *Appl. Opt*., vol. 48, no. 30, pp. 5748–5758, 2009.

[65] A. Kannath, J. Hodgkinson, R. G. Gillard, R. J. Riley, and R. P. Tatam, "A VCSEL based system for on-site monitoring of low level methane emission," in *Proc. SPIE*, vol. 7952, pp. 79520F, 2011.

[66] K. Bamford, H. Barr, and R. P. Tatam, "Optical low coherence tomography of bronchial tissue," in *Proc. SPIE*, vol. 3858, pp. 172–179, 1999.

[67] P. Casaubieilh, H. D. Ford, and R. P. Tatam, "Optical fiber Fizeau-based OCT, " in *Proc. SPIE*, vol. 5502, pp. 338–341, 2004.

[68] K. Bamford, J. James, H. Barr, and R. P. Tatam, "Radar detection of precancerous bronchial tissue," *Lasers in Medical Science*, vol. 15, no. 3, pp. 188–194, 2000.

[69] H. D. Ford, R. Beddows, P. Casaubieilh, and R. P. Tatam, "Comparative signal-to-noise analysis of fiber-optic based OCT systems," *J. of Mod. Opt*., vol. 52, no. 14, pp 1965–1979, 2005.

[70] H. D. Ford and R. P. Tatam, "Fiber imaging bundles for full-field optical coherence tomography," *Meas. Sci. Technol.*, vol. 18**,** no. 9, pp.2949–2957, 2007.

[71] A. Saglam, H. D. Ford, and R. P. Tatam, "Numerical modelling of imaging fiber bundles and their application in optical coherence tomography," in *Proc. SPIE*, vol. 7753, pp. 775350 (4 pages), 2011.

[72] H. D. Ford and R. P. Tatam, "Characterization of optical fiber imaging bundles for swept-source OCT," *Appl. Opt.*, vol. 50, no. 5, pp. 627–640, 2011.

[73] H. D. Ford, R. P. Tatam, S. Landahl, and L. Terry, "Investigation of disease in stored onions using optical coherence tomography," presented at *ISHS Postharvest Unlimited (paper no. A7-42011)*, Leavnworth, WA, USA, May 23–26, 2011.

[74] C. J. Duffy and R. P. Tatam, "Optical heterodyne carrier generation utilizing stimulated Brillouin scattering in birefringent optical fiber," *Electron. Letts.*, vol. 27, no. 22, pp. 2004–2006, 1991.

[75] C. J. Duffy and R. P. Tatam, "Optical frequency shifter technique based on stimulated Brillouin scattering in birefringent optical fiber," *Appl. Opt.*, vol. 32, no. 30, pp. 5966–5972, 1993.

[76] O. S. Khan and R. P. Tatam, "Optical frequency shifter based on stimulated Brillouin scattering in a birefringent optical fiber ring resonator," *Opt. Commun*., vol. 103, no. 1–2, pp. 161–168, 1993.

[77] H. D. Ford and R. P. Tatam, "Polarization-based optical fiber wavelength filters," *J. Lightwave Technol*., vol. 13, .no. 7, pp. 1435–1444, 1995.

[78] H. D. Ford and R. P. Tatam, "Multiplexed sensor network employing birefringent fiber WDM's," *Opt. Commun*., vol. 131, no. 4–6, pp 290–294, 1996.

[79] A. Ezbiri and R. P. Tatam, "Passive signal processing for a miniature Fabry-Perot interferometric sensor using a multimode laser diode source," *Opt. Lett.*, vol. 20, no. 17, pp. 1818–1820, 1995.

[80] A. Ezbiri and R. P. Tatam, "Interrogation of low finesse optical fiber Fabry-Perot interferometers using a four wavelength technique," *Meas. Sci. Technol.*, vol. 7, no. 2, pp. 117–120, 1996.

[81] A. Ezbiri and R. P. Tatam, "Five wavelength interrogation technique for miniature fiber optic Fabry-Perot sensors," *Opt. Commun*., vol. 133, no. 1–6, pp. 62–66, 1997.
[82] J. Potter, A. Ezbiri, and R. P. Tatam, "A broad band signal processing technique for miniature low-finesse Fabry-Perot interferometric sensors," *Opt. Commun*., vol. 140, no. 1–3, pp. 11–14, 1997.
[83] R. B. Charters, A. Kuczynski, S. E. Staines, R. P. Tatam, and G. J. Ashwell, "In-line fiber optic channel dropping filter using Langmuir-Blodgett films," *Electron. Letts.*, vol. 30, no. 7, pp. 594–595, 1994.
[84] R. B. Charters, S. E. Staines, and R. P. Tatam, "In-line fiber-optic components using Langmuir-Blodgett films," *Opt. Letts*., vol. 19, no. 23, pp. 2036–2038, 1994.
[85] D. Flannery, S. W. James, R. P. Tatam, and G. J. Ashwell, "pH Sensor using Langmuir-Blodgett overlays on polished optical fiber," *Opt. Lett.*, vol. 22, no. 8, pp. 567–569, 1997.
[86] D. Flannery, S. W. James, R. P. Tatam, and G. J. Ashwell, "Fiber optic chemical sensing using Langmuir-Blodgett overlay waveguides," *Appl. Opt.*, vol. 38, no. 36, pp. 7370–7374, 1999.
[87] G. J. Ashwell, G. Jefferies, C. D. George, R. Ranjan, R. B. Charters, and R. P. Tatam, "Z-type Langmuir-Blodgett film structures: surface plasmon resonance, second harmonic generation and fiber optic devices," *J. Mat. Chem*., vol. 6**,** no. 2, pp. 131–136, 1996.
[88] S. S. Johal, S. E. Staines, S. W. James, R. P. Tatam, and G. J. Ashwell, "A technique for depositing non-centrosymmetric Langmuir-Blodgett films onto optical fiber," *Meas. Sci. Technol.*, vol. 10, no. 5, pp. N60–N62, 1999.
[89] S. S. Johal, S. W. James, R. P. Tatam, and G. J. Ashwell, "Second-harmonic-generation in Langmuir-Blodgett waveguide overlays on single mode optical fiber," *Opt. Lett.*, vol. 24, no. 17, pp. 1194–1196, 1999.
[90] N. D. Rees, S. W. James, S. E. Staines, G. J. Ashwell, and R. P. Tatam, "Submicrometer fiber optic Fabry-Perot interferometer formed by the use of the Langmuir-Blodgett technique," *Opt. Lett.*, vol. 26, no. 23, pp. 1840–1842, 2001.
[91] M. L. Dockney, S. W. James, and R. P. Tatam, "Fiber Bragg gratings fabricated using a wavelength tuneable laser source and a phase mask based interferometer," *Meas. Sci. Technol*., vol. **7**, no. 4, pp. 445–448, 1996.
[92] S. W. James, M. L. Dockney, and R. P. Tatam, "Photorefractive volume holographic demodulation of in-fiber Bragg grating sensors," *IEEE Photon. Technol. Letts*., vol. 8, no. 5, pp. 664–666, 1996.
[93] C. K. Chatterjea, S. W. James, and R. P. Tatam, "Pseudo-heterodyne signal processing scheme for interrogation of fiber Bragg grating sensor arrays," in *Proc. SPIE*, vol. 3478, pp. 266–274, 1998.
[94] S. W. James, M. L. Dockney, and R. P. Tatam, "Simultaneous independent temperature and strain measurement using in-fiber Bragg grating sensors," *Electron. Letts*., vol. 32, no 12, pp. 1133–1134, 1996.
[95] A. Wilson, S. W. James, and R. P. Tatam, "Time-division-multiplexed interrogation of fiber Bragg grating sensors using laser diodes," *Meas. Sci. Technol*., vol. 12, no. 2, pp. 181–187, 2001.
[96] E. Chehura, S. W. James, and R. P. Tatam, "Temperature and strain discrimination using a single tilted fiber Bragg grating," *Opt. Commun.*, vol. 275, no. 2, pp. 344–347, 2007.
[97] S. P. Reilly, S. W. James, and R. P. Tatam, "Tuneable and switchable dual wavelength lasers using optical fiber Bragg grating external cavities," *Electron. Letts.*, vol. 38, no. 18, pp.1033–1034, 2002.
[98] S. W. James, C. C. Wei, C. C. Ye, R. P. Tatam, and P. E. Irving, "An investigation of the tensile strength of fiber Bragg gratings," in *Proc. SPIE*, vol. 3746, pp. 38–41, 1999.
[99] C. Y. Wei, C. C. Ye, S. W. James, P. E. Irving, and R. P. Tatam, "AFM observation of surface topography of fiber Bragg gratings fabricated in germanium-boron codoped fibers and hydrogen-loaded fibers," *Opt. Mat*., vol. 20, no. 4, pp. 283–294, 2002.
[100] C. Y. Wei, C. C. Ye, S. W. James, R. P. Tatam, and P. E. Irving, **"**The influence of hydrogen lading and the fabrication process on the mechanical strength of optical fiber Bragg gratings," *Opt. Mat*., vol. 20, no. 4, pp. 241**–**251, 2002.
[101] M. J. O'Dwyer, S. W. James, C. C. Ye, and R. P. Tatam, "Thermal dependence of the strain response of optical fiber Bragg gratings," *Meas. Sci. Technol*., vol. 15, no. 8, pp. 1607–1613, 2004.
[102] M. J. O'Dwyer, N. D. Dykes, S. W. James, R. P. Tatam, and P. E. Irving, "Impact detection in carbon fiber reinforced polymer composites using in-fiber Bragg gratings," in *Proc. SPIE*, vol. 3479, pp. 192–199, 1998.
[103] C. Y. Wei, S. W. James, C. C. Ye, R. P. Tatam, and P. E. Irving, "Application issues using fiber Bragg gratings as strain sensors in fiber composites," *Strain*, vol. 36, no. 3, pp.143–150, 2000.
[104] R. M. Groves, E. Chehura, W. Li, S. W. James, and R. P. Tatam, "Surface strain measurement: a comparison of speckle shearing interferometry and optical fiber Bragg gratings with resistance foil strain gauges," *Meas. Sci. Technol.*, vol. 18, no. 5, pp. 1175–1184, 2007.
[105] M. J. O'Dwyer, G. M. Maistros, S. W. James, R. P. Tatam, and I. K. Partridge, "Relating the state of cure to real time internal strain development in a curing composite using in-fiber Bragg gratings and dielectric sensors," *Meas. Sci. Technol*., vol. 9, no. 8, pp. 1153–1158, 1998.

[106] E. Chehura, A. A. Skordos, C. C. Ye S. W. James, I. K. Partridge, and R. P. Tatam, "Strain development in curing epoxy resin and glass fiber/epoxy composites monitored by fiber Bragg grating sensors in birefringent optical fiber," *Smart Materials and Structures*, vol. 14, no. 2, pp. 354–362, 2005.

[107] S. J. Buggy, E. Chehura, S. W. James, and R. P. Tatam, "Optical fiber grating refractometers for resin cure monitoring," *J. Opt. A: Pure and Appl. Opt.*, vol. 9, no. 6, pp. S60–S65, 2007.

[108] A. Dimopoulos, S. J. Buggy, A. A. Skordos, S. W. James, R. P. Tatam, and I. K. Partridge, "Monitoring cure in epoxies containing carbon nanotubes using an optical fiber Fresnel refractometer," *J Appl. Poly. Sci*., vol. 113, no. 2, pp. 730–735, 2009.

[109] G. Dell'anno, I. K. Partridge, D. D. R. Cartie, A. Hamlyn, E. Chehura, S. W. James, R. P. Tatam, and R. Lefrancois, "ADVITAC: automated manufacture of 3-D reinforced aerospace structures," presented at *the 1st European Aeronautics Science Network (EASN) workshop on Aerostructures*, Paris, France, October, 2010.

[110] S. W. James, R. P. Tatam, A. Twin, M. Morgan, and P. Noonan, "Strain response of fiber Bragg grating sensors at cryogenic temperatures," *Meas. Sci. Technol*., vol. 13, no. 10, pp. 1535–1539, 2002.

[111] E. Chehura, S. W. James, A. Twin, F. Domptail, and R. P. Tatam, "Multicomponent strain development in superconducting magnet coils using optical fiber grating sensors fabricated in highly linearly birefringent fiber," in *Proc. SPIE*, vol. 7503, pp. 75035J (4 pages), 2009.

[112] C. C. Ye and R. P. Tatam, **"**Ultrasonic sensing using Yb^{3+}/Er^{3+}- codoped distributed feedback fiber grating lasers," *Smart Materials and Structures*, vol. 4, no. 1, pp. 170**–**176, 2005.

[113] S. W. James, R. P. Tatam, S. J. Fuller, and C. Crompton, "Monitoring transient strain on a gun barrel using in-fiber Bragg grating sensors," *Meas. Sci. Technol.*, vol. 10, no. 2, pp. 63–67, 1999.

[114] S. W. James, S. F. M. Chastin, R. P. Tatam, and G. Boulton, "Geoptical spline: Soil and sediment deformation sensor," in *Proc*. *IEICE*, pp.140–143, 2003.

[115] J. Li, R. Correira, E. Chehura, S. Staines, S. W. James, and R. P. Tatam, "A fiber Bragg grating based inclinometer system for ground movement measurement," in *Proc. SPIE*, vol. 7653, pp. 765314-1–765314-4, 2010.

[116] J. Li, R. Correia, E. Chehura, S. Staines, S. W. James, R. P. Tatam, A. P. Butcher, and R. Fuentes, "Field monitoring of static, dynamic and statnamic pile loading tests using fiber Bragg grating strain sensors," in *Proc. SPIE*, vol. 7503, pp. 75034O-1–75034O-4, 2009.

[117] E. Chehura, S. W. James, N. Lawson, K. P. Garry, and R. P. Tatam, "Pressure measurements on aircraft wing using phase-shifted fiber Bragg grating sensors," in *Proc. SPIE*, vol. 7503, pp. 750334 (4 pages), 2009.

[118] S. J. Buggy, S. W. James, S. Staines, R. Carroll, P. Kitson, and R. P. Tatam, "Continuous non-destructive optical monitoring of in-situ fishplated joints," presented at *Railway Engineering Conference*, London, June 29–30, 2011.

[119] R. N. Correia, E. Chehura, S. W. James, and R. P. Tatam, "Locally transverse loaded fiber Bragg grating for pressure sensing applications," *Meas. Sci. Technol*., vol. 18, no. 10, pp. 3101–3110, 2007.

[120] R. N. Correia, J. Li, E. Chehura, S. W. James, and R. P. Tatam, "A new transverse loading packaging technique to enhance the load measurement capability of fiber Bragg gratings," *Meas. Sci. Technol*., vol. 21, no. 9, article no. 094006 (7 pages), 2010.

[121] E. Chehura S. W. James, and R. P. Tatam, "A simple and wavelength-flexible procedure for fabricating phase-shifted fiber Bragg gratings," *Meas. Sci. Technol*., vol. 21, no. 9, article no. 94001 (7 pages), 2010.

[122] R. Correia, J. Li, S. Staines, E. Chehura, S. W. James, J. Kutner, P. Dewhurst, P. Ferreira, and R. P. Tatam, "Fiber Bragg grating based effective soil pressure sensor for geotechnical applications," in *Proc. SPIE*, vol. 7503, pp. 75030F-1–75030F-4, 2009.

[123] C. C. Ye, S. E. Staines, S. W. James, and R. P. Tatam, "A polarization maintaining fiber Bragg grating interrogation system for multi-axis strain sensing," *Meas. Sci. Technol*., vol. 13 , no. 9, pp. 1446–1449, 2002.

[124] G. Gagliardi, M. Salza, P. Ferraro, E. Chehura, R. P. Tatam, T. K. Gangopadhyay, N. Ballard, D. Paz-Soldan, J. A. Barnes, H. P. Loock, T. T. Y. Lam, J. H. Chow, and P. De Natale, "Optical fiber sensing based on reflection laser spectroscopy," *Sensors*, vol. 10, no. 3, pp. 1823–1845, 2010.

[125] E. Chehura, C. C. Ye, S. E. Staines, S. W. James, and R. P. Tatam, **"**Characterization of the response of fiber Bragg gratings fabricated in stress and geometrically induced high birefringent fibers to temperature and transverse load," *Smart Mat. & Struct.*, vol. 13, no. 4, pp. 888**–**895, 2004.

[126] C. C. Ye, S. W. James, and R. P. Tatam, **"**Simultaneous temperature and bend sensing using long period fiber gratings," *Opt. Lett.*, vol. 25, no. 14, pp. 1007**–**1009, 2000.

[127] S. Khaliq, S. W. James, and R. P. Tatam, **"**Fiber optic liquid level sensor using a long period grating," *Opt. Lett*., vol. 26, no. 16, pp. 1224**–**1226, 2001.

[128] S. Khaliq, S. W. James, and R. P. Tatam, "Enhanced sensitivity fiber optic long period grating temperature sensor," *Meas. Sci. Technol*., vol. 13, no. 5, pp 792–795, 2002.

[129] S. W. James, R. P. Tatam, A. Twin, R. Bateman, and P. Noonan, **"**Cryogenic temperature response of fiber optic long period gratings," *Meas. Sci. Technol*., vol. 14, no. 8, pp. 1409**–**1411, 2003.

[130] S. W. James and R P. Tatam, **"**Optical fiber long period grating sensors: characteristics and application," *Meas. Sci. Technol*., vol. 14, no. 5, pp. R49**–**R61, 2003.

[131] R. P. Murphy, S. W. James, and R. P. Tatam, "Multiplexing of fiber optic long period grating based interferometric sensors," *J. Lightwave Technol.*, vol. 25, no. 3, pp. 825–829, 2007.

[132] S. W. James, I. Ishaq, G. J. Ashwell, and R. P. Tatam, "Cascaded long period gratings with nano-structured coatings," *Opt. Lett.*, vol. 30, no. 17, pp. 2197–2199, 2005.

[133] I. Ishaq, S. W. James, G. J. Ashwell, and R. P. Tatam, "Modification of the refractive index response of long period gratings using thin film overlays," *Sens. & Act. B: Chem.*, vol. 107, no. 2, pp. 738–741, 2005.

[134] S. W. James and R. P. Tatam, "Fiber optic sensors with nano-structured coatings," *J. Opt. A: Pure Appl. Opt.*, vol. 8, no. 7, pp. S430–S444, 2006.

[135] S. W. James, C. S. Cheung, and R. P. Tatam, "Experimental observations on the response of 1st and 2nd order fiber optic long period grating coupling bands to the deposition of nanostructured coatings," Opt. Express, vol. 15, no. 20, pp. 13096–13107, 2007.

[136] S. C. Cheung, S. M. Topliss, S. W. James, and R. P. Tatam, "Response of fiber optic long period gratings operating near the phase matching turning point to the deposition of nanostructured coatings," *J. Opt. Soc. Am. B*, vol. 25, no. 6, pp. 897–902, 2008.

[137] S. M. Topliss, S. W. James, F. Davis, S. J. P. Higson, and R. P. Tatam, "Optical fiber long period grating based selective vapour sensing of volatile organic compounds," *Sensors Actuators B: Chem.*, vol. 143, no. 2, pp. 629–634, 2010.

[138] S. Korposh, S. W. James, S. W. Lee, S. M. Topliss, S. C. Cheung, W. J. Batty, and R. P. Tatam, "Fiber optic long period grating sensors with a nanoassembled mesoporous film of SiO_2 nanoparticles," *Opt. Express.*, vol. 18, no. 12, pp. 13227–13238, 2010.

[139] R. Jarzebinska, S. W. James, and R. P. Tatam, "Response of the transmission spectrum of tapered optical fibers to the deposition of a nanostructured coating," *Meas. Sci. Technol*., vol. 20, no. 3, article no. 034001 (6 pages), 2009.